Chem Soc Rev

Chemical Society Reviews

www.rsc.org/chemsocrev

Volume 40 | Number 6 | June 2011 | Pages 3053–3368

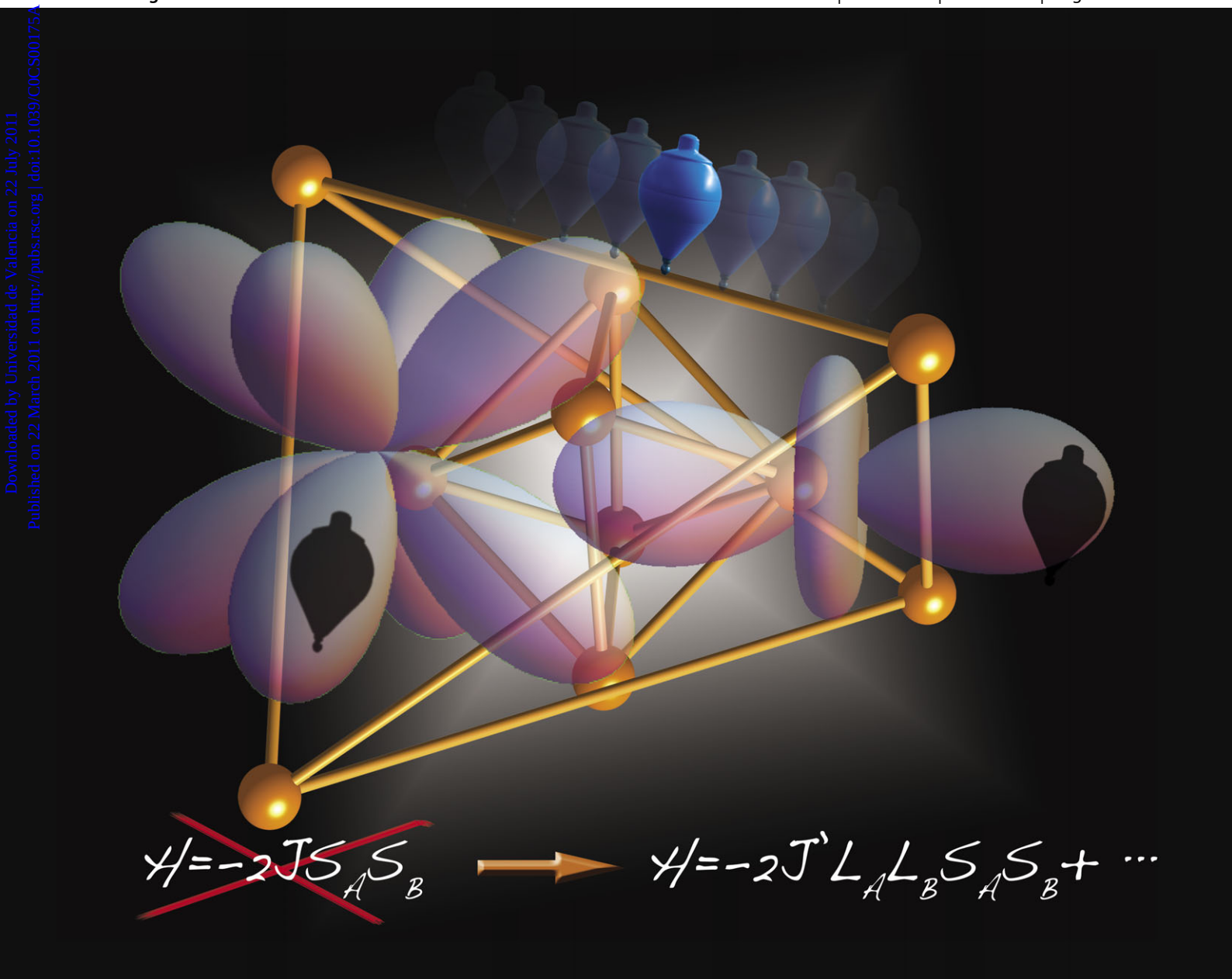

Themed issue: Molecule-based magnets

ISSN 0306-0012

RSC Publishing

CRITICAL REVIEW

Andrei Palii, Boris Tsukerblat, Sophia Klokishner, Kim R. Dunbar, Juan M. Clemente-Juan and Eugenio Coronado
Beyond the spin model: exchange coupling in molecular magnets with unquenched orbital angular momenta

Chem Soc Rev

This article was published as part of the

Molecule-based magnets themed issue

Guest editors Joel S. Miller and Dante Gatteschi

Please take a look at the issue 6 2011 table of contents to access other reviews in this themed issue

Chem Soc Rev

View Online
Dynamic Article Links

Cite this: *Chem. Soc. Rev.*, 2011, **40**, 3130–3156

www.rsc.org/csr

CRITICAL REVIEW

Beyond the spin model: exchange coupling in molecular magnets with unquenched orbital angular momenta†

Andrei Palii,*[a] Boris Tsukerblat,*[b] Sophia Klokishner,[a] Kim R. Dunbar,[c] Juan M. Clemente-Juan[d] and Eugenio Coronado[d]

Received 10th November 2010
DOI: 10.1039/c0cs00175a

In this *critical review* we review the problem of exchange interactions in polynuclear metal complexes involving orbitally degenerate metal ions. The key feature of these systems is that, in general, they carry an unquenched orbital angular momentum that manifests itself in all their magnetic properties. Thus, interest in degenerate systems involves fundamental problems related to basic models in magnetism. In particular, the conventional Heisenberg–Dirac–Van Vleck model becomes inapplicable even as an approximation. In the first part we attempt to answer two key questions, namely which theoretical tools are to be used in the case of degeneracy, and how these tools can be employed. We demonstrate that the exchange interaction between orbitally degenerate metal ions can be described by the so-called orbitally-dependent exchange Hamiltonian. This approach has shown to reveal an anomalously strong magnetic anisotropy that can be considered as the main physical manifestation of the unquenched orbital angular momentum in magnetic systems. Along with the exchange coupling, a set of other interactions (such as crystal field effects, spin–orbit and Zeeman coupling), which are specific for the degenerate systems, need to be considered. All these features will be discussed in detail using a pseudo-spin-1/2 Hamiltonian approach. In the second part, the described theoretical background will be used to account for the magnetic properties of several magnetic metal clusters and low-dimensional systems: (i) the dinuclear face-sharing unit $[Ti_2Cl_9]^{3-}$, which exhibits a large magnetic anisotropy; (ii) the rare-earth compounds $Cs_3Yb_2Cl_9$ and $Cs_3Yb_2Br_9$, which, surprisingly, exhibit a full magnetic isotropy; (iii) a zig-zag Co^{II} chain exhibiting unusual combination of single-chain magnet behavior and antiferromagnetic exchange coupling; (iv) a trigonal bipyramidal Ni_3Os_2 complex; (v) various Co^{II} clusters encapsulated by polyoxometalate ligands. In the two last examples a pseudospin-1/2 Hamiltonian approach is applied to account for the presence of exchange anisotropy (150 references).

1. Introduction

Molecular magnetism represents a fascinating interdisciplinary field of research that incorporates basic concepts of physics, chemistry and materials science. The evolution of this field is described in detail in several papers and books[1,2] and the contemporary state-of-the-art is summarized in the recent book of Gatteschi *et al.*[1] The main objects of molecular magnetism are either magnetic molecules consisting of a finite number of exchange coupled spin sites (molecular magnetic clusters) or extended materials based on magnetic molecules (molecule-based magnets).[1–23] Some important materials in this context are the so-called single molecule magnets and single chain magnets (SMMs and SCMs),[23–32] the high T_c molecule-based ferromagnets[33–41] and the multifunctional magnetic materials.[42–52] Organic molecules of increasing sizes and large numbers of unpaired electrons are also being explored as building blocks for molecular-based magnets.[53–59] Possible applications of these materials are for use as memory storage units of molecular size,[1–3] as carriers of quantum bits of information[60–77] and as components of spintronic devices.[78]

Let us now focus on the molecular magnetic clusters. Apart from their interest as SMMs, and in biophysics/biochemistry,[79–82] these clusters have been shown to represent ideal model systems for studying the exchange interactions at the molecular

[a] *Institute of Applied Physics, Academy of Sciences of Moldova, Academy Str. 5, MD 2028 Kishinev, Moldova. E-mail: andrew.palii@uv.es*
[b] *Department of Chemistry, Ben-Gurion University of the Negev, P.O. Box 653, Beer-Sheva 84105, Israel. E-mail: tsuker@bgu.ac.il*
[c] *Department of Chemistry, Texas A&M University, College Station, TX 77843, USA*
[d] *Instituto de Ciencia Molecular, Universidad de Valencia, Polígono de la Coma, s/n 46980 Paterna, Spain*
† Part of the molecule-based magnets themed issue.

scale. Over the course of several decades, the exchange interactions in these clusters have been modeled using the Heisenberg–Dirac–Van Vleck (HDVV) Hamiltonian. This Hamiltonian is expressed in terms of spin operators and strictly speaking it is applicable to clusters composed by magnetic centers having isolated ground spin states. The

Andrei Palii

Andrei Palii received his PhD from the University of Riga in 1990 under the supervision of Professor Boris Tsukerblat. He carried out post-doctoral research with Professor Eugenio Coronado at the University of Valencia. In 2007 Andrei Palii was habilitated from the Institute of Applied Physics of the Academy of Sciences of Moldova, where he is now a Chief Researcher. His current interests include the study of orbital effects in single-molecule magnets and single-chain magnets, and electron delocalization and magnetic interactions in mixed-valence compounds.

Boris Tsukerblat

Boris Tsukerblat is Professor of the Chemistry Department of the Ben-Gurion University of the Negev in Israel, Beer-Sheva. He obtained his scientific degrees of Candidate of Sciences (Ph.D.) in theoretical physics from the Kazan State University, Russia, and habilitation (Doctor of Sciences) from the State University of Tartu, Estonia. He headed the molecular magnetism group at the Institute of Chemistry and Institute of Applied Physics of the Academy of Sciences of Moldova. He is a Corresponding Member of this Academy. His scientific interests are focused on molecular magnetism including exchange interactions, single-molecule magnets, mixed valency, double exchange, group-theoretical and computational approaches, vibronic interactions and Jahn–Teller effect in molecules and solids.

Sophia Klokishner

Sophia Klokishner is the head of the Department of Ternary and Multinary Compounds at the Institute of Applied Physics of the Academy of Sciences of Moldova. She obtained her PhD at the State University of Moldova in 1978 and habilitated in 1994 at the Institute of Applied Physics. Her main research interests are theoretical aspects of molecular magnetism, Jahn–Teller effect and vibronic interactions in molecules and solids, cooperative phenomena in solids, spectroscopy of doped crystals.

Kim R. Dunbar

Kim R. Dunbar was born in Mount Pleasant, PA, and received a BS degree from Westminster College in 1980 and a PhD from Purdue University in 1984. After a postdoctoral stint at Texas A&M University, she joined the faculty of Michigan State University in 1987 and moved to Texas A&M University in 1999, where she is a Distinguished Professor and holds the Davidson Chair of Science. Her research spans topics in synthetic and structural inorganic chemistry, with a focus on the design of conducting and magnetic molecular materials, supramolecular anion interactions, and the anticancer properties of metal complexes. She is a Fellow of the American Association for the Advancement of Science, and a past Fellow of the Alfred P. Sloan Foundation and a Camille and Henry Dreyfus Teacher–Scholar. She received Distinguished Alumna Awards from Westminster College in 2000 and Purdue University in 2004, and a Distinguished Faculty Award from Michigan State University in 1998. In 2006 she received the Inaugural Distinguished Award from the Association of Former Students at Texas A&M University for Graduate Mentoring. She is an Associate Editor for the ACS journal Inorganic Chemistry and has served as Chair and Secretary of the ACS Division of Inorganic Chemistry.

systems of this kind can be referred to as *spin clusters*. The key physical feature of the HDVV interaction is that it is magnetically isotropic. In general, the anisotropy in spin clusters is relatively small in the sense that the parameters of the anisotropic interactions are much smaller as compared to those involved in the HDVV coupling. Nevertheless, there is a second type of systems, which involves clusters comprising magnetic ions with orbitally degenerate ground crystal field terms. For the sake of brevity they will be referred to as *degenerate clusters*. In contrast to the exchange interaction in spin clusters, the magnetic coupling in these clusters cannot be described in terms of spin operators only (with the exception of some special cases). In fact, the exchange Hamiltonian has a much more complicated form that includes orbital variables along with spin operators. In general, the orbital degeneracy is directly related to an unquenched orbital angular momentum in the electronic shell that will be shown to manifest itself in a strong magnetic anisotropy. It is to be noted that the anisotropic interactions in systems composed of ions with unquenched orbital angular momenta are of the same order of magnitude as the isotropic ones.

The theoretical background of molecular magnetism dealing with spin-clusters is highly developed and has been described in detail in many reviews and books.[1–7,14–20] On the contrary, the problem of orbital degeneracy has not received much attention in the field of molecular magnetism in spite of its fundamental and practical importance. Moreover, due to its conceptual simplicity and the availability of efficient computer programs adapted to spin-systems, the HDVV model is frequently used in molecular magnetism even for those cases for which it is inapplicable even as an approximation. In these cases, however the parameters resulting from fitting the experimental data to the theoretical data derived from the spin model turn out to be artificial. On the other hand, a detailed description of the orbitally-degenerate systems is much more complicated, and often requires the use of complementary experimental techniques (magnetic as well as spectroscopic) in order to obtain reliable information about the large number of electronic and magnetic parameters. For this reason few efforts have been devoted to the modeling of these systems in a rigorous fashion.

In this review we will show that, in spite of the internal complexity of the exchange problem in degenerate systems, one can often gain insight into their key features even without applying complicated theoretical approaches, but rather by using only basic quantum-mechanical methods such as perturbation theory and simple orbital schemes supplemented by the symmetry arguments. It turns out, that the imaginative orbital pictures can guide the reader through the subsequent analysis of more complicated molecular clusters that are of current interest in molecular magnetism.

Although the ability of the orbitally-dependent magnetic interactions to create strong magnetic anisotropy was mentioned in general terms many years ago by Van Vleck,[83] this phenomenon has not been understood to any great extent until the last decade and consequently the topic has not explored in molecular magnetism. The present review article is an attempt to give a description of this kind of phenomenon in the context of its relevance to the contemporary problems of molecular magnetism. The review summarizes the conceptual aspects of the theory of magnetic exchange in degenerate systems and its applications to describe the properties of molecular magnets. Along with the general ideas and applications, we also provide the reader with a few details on the calculations in some simple cases for which a quantitative analysis of the data is possible. This will permit the reader to avoid (at least, in most cases) the reading of numerous original papers.

The review paper is organized as follows. We begin with Anderson's basic concept of the kinetic exchange which leads to the isotropic HDVV model of the exchange interaction (Section 2). In Section 3 we discuss the inapplicability of

Juan Modesto Clemente-Juan

Juan M. Clemente-Juan received his PhD in Chemistry in 1998 at the Universidad de Valencia under the supervision of Prof. E. Coronado and Dr J.J. Borrás-Almenar. From 1998 to 2001 he was a post-doctoral researcher in the group of Prof. J.P. Tuchagues. Since 2001 he has been a researcher at ICMol (Universidad de Valencia). His research interests cover different aspects of molecular magnetism: exchange-coupled and single ion SMM and mixed valence systems.

Eugenio Coronado

Eugenio Coronado is Director of the Institute of Molecular Science at the Valencia University (ICMol) and Scientific Director of the European Institute of Molecular Magnetism (EIMM). His research interests lie in the area of molecular magnetism, where he has made both theoretical and experimental contributions. From a theoretical point of view his work has focused on the modelling of the magnetic properties of high-nuclearity magnetic clusters and low-dimensional magnetic materials, as well as in the development of the computing programs MAGPACK and MVPACK. From the experimental point of view he has been interested in the design and study of multifunctional molecular materials and molecular nanomagnets.

the conventional isotropic HDVV Hamiltonian to model the exchange interaction between orbitally degenerate metal ions that possess unquenched orbital angular momenta. In Section 4 we introduce the concept of orbitally-dependent exchange and deduce, for a particular case, the orbitally-dependent anisotropic exchange Hamiltonian using a second-order perturbation approach. Next we demonstrate that, in some special cases, the exchange between orbitally-degenerate ions can be isotropic and is described by the pseudo-HDVV orbitally-independent exchange Hamiltonian. Finally, we consider the case of strong spin–orbit (SO) coupling and establish a microscopic background for the pseudo-spin-1/2 Hamiltonian that is widely used for the description of the effective interaction involving the ground Kramers doublets (for example, in cobalt(II) systems). Section 5 illustrates some applications of the theory. The orbitally-dependent exchange and magnetic anisotropy of the $[Ti_2Cl_9]^{3-}$ unit in the $Cs_3Ti_2Cl_9$ crystalline compounds are discussed. The orbitally-dependent exchange is considered in the rare-earth compounds. Specifically, for the materials $Cs_3Yb_2Cl_9$ and $Cs_3Yb_2Br_9$ the origin of surprising isotropy of this interaction is revealed. The pseudo-spin-1/2 Hamiltonian approach is applied to reveal the origin of SCM behavior of the antiferromagnetic zig-zag chain compound based on $Co(H_2L)(H_2O)$ units, and to the study of the magnetic properties of the trigonal bipyramidal Ni_3Os_2 complex. This approach is also illustrated by the combined data from the inelastic neutron scattering spectra, magnetic susceptibility and specific heat measurements in polyoxometalates encapsulating Co^{II} clusters of increasing nuclearities. The main results and perspective for the field are summarized in the concluding part of the review.

2. Basic concepts: Anderson's model for the kinetic exchange and Heisenberg–Dirac–Van Vleck Hamiltonian

The basic concepts of the microscopic theory of magnetic exchange can be illustrated by considering the spin-clusters in which the ground terms of the constituent metal ions are orbitally non-degenerate. It is conventional to distinguish the two main mechanisms of the exchange interaction, namely, *kinetic and potential*. The potential exchange is described in all textbooks on quantum mechanics and quantum chemistry so we will focus only on the kinetic exchange mechanism that in most cases is dominating in the metal clusters.

We start with the concept of the kinetic exchange in a simplest case of exchange-coupled pair of the metal ions A and B, when each ion possesses one unpaired electron occupying a non-degenerate orbital φ_i (i = A, B). Usually, the magnetic exchange between the metal ions is mediated by the bridging diamagnetic atoms (ligands), and, for this reason, such coupling is called superexchange. The basic idea of the kinetic superexchange proposed by Anderson[84,85] is that the unpaired electrons are not fully localized on the metal ions and some non-vanishing spin densities can be found on the bridging ligands due to covalency. Then,

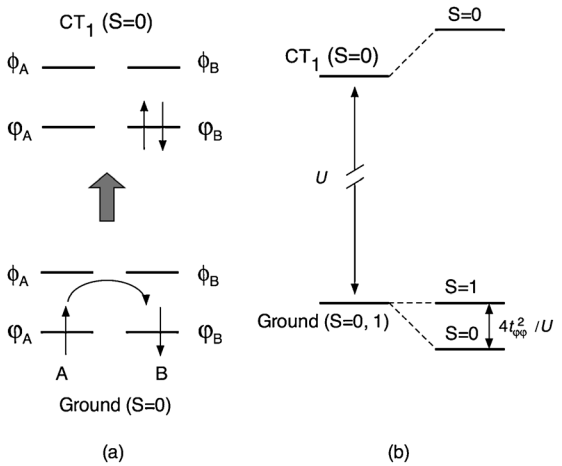

Fig. 1 Schematic diagram for the mechanism of the antiferromagnetic kinetic exchange: (*a*) orbital population in the ground spin-singlet state (one microstate contributing to this state) and one CT_1 configuration; (*b*) full spin states and exchange splitting.

the one-electron wave-functions describing these electrons (magnetic orbitals) are mainly of 3d-character but include also some admixture of the bridging s and p-orbitals.

Virtual electron transfer that mixes the ground state of the dimer with the excited charge-transfer (CT) states is mainly caused by the kinetic energy of the electrons which justifies the term kinetic exchange. This electron transfer gives rise to a second-order spin-dependent splitting. Fig. 1 and 2 illustrate different kinetic exchange mechanisms. The system under consideration is assumed to consist of the two identical one electron ions A and B whose energy patterns involve two energy levels with the corresponding orbitals φ_A,ϕ_A and φ_B,ϕ_B (Fig. 1 and 2). It is also supposed that the energy gap Δ between these two levels considerably exceeds all inter-center exchange interactions and in the ground state of the system only the low lying levels are populated. According to Anderson's concept one should consider two types of the CT configurations that give rise to two distinct mechanisms of the kinetic exchange: (1) CT between the half-filled orbitals (Fig. 1) and (2) CT from the half-filled to empty orbitals (Fig. 2). The ground manifold of the pair includes the following four microstates corresponding to four different spin orientations of spins occupying two orbitals of different centers: $\uparrow\uparrow(M_S = 1, S = 1)$; $\uparrow\downarrow,\downarrow\uparrow(M_S = 0, S = 1,0)$; $\downarrow\downarrow(M_S = -1, S = 1)$ where M_S is the quantum number of the total spin-projection of the dimer. The wave-functions of the pair corresponding to these microstates should be expressed in terms of Slater determinants in order to meet the requirements of Pauli principle: $|\uparrow\uparrow, M_S = 1\rangle = |\varphi_A\varphi_B|$, $|\uparrow\downarrow, M_S = 0\rangle = |\varphi_A\bar{\varphi}_B|$, $|\downarrow\uparrow, M_S = 0\rangle = |\bar{\varphi}_A\varphi_B|$, $|\downarrow\downarrow, M_S = -1\rangle = |\bar{\varphi}_A\bar{\varphi}_B|$ where $|\ldots|$ is the sign of determinant, φ_i and $\bar{\varphi}_i$ are the spin-orbitals (for the sake of simplicity the orbitals are assumed to be orthogonal) with spin up and down respectively ($\varphi_i \equiv |\varphi_i(\boldsymbol{r})\uparrow\rangle$ and $\bar{\varphi}_i \equiv |\varphi_i(\boldsymbol{r})\downarrow\rangle$). From these microstates one can build the wave-functions $\Psi_{gr}(S,M_S)$ which are characterized by the quantum numbers of the total spin of the dimer S and its projection M_S. The ground terms of the dimer are the spin-singlet ($S = 0$) and spin-triplet

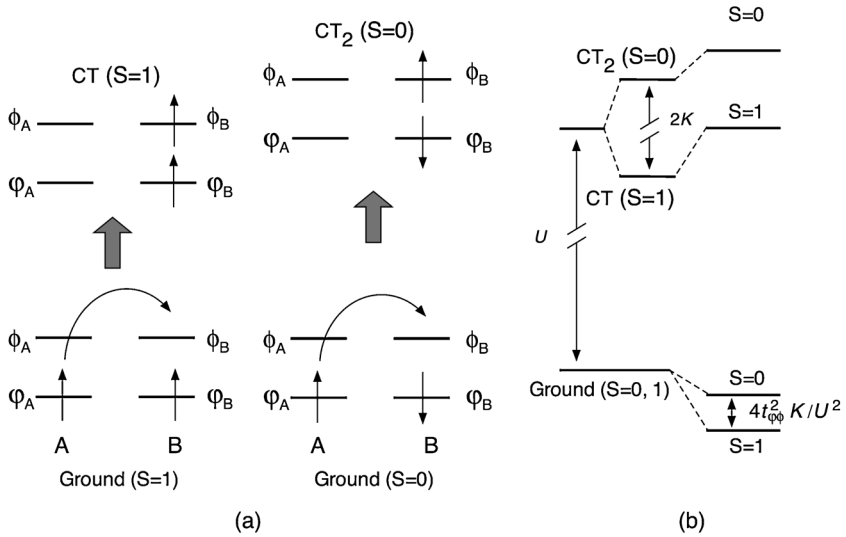

Fig. 2 Schematic diagram for the mechanism of the ferromagnetic kinetic exchange: (*a*) orbital populations in the ground and CT configurations; (*b*) full spin states and exchange splitting. Adapted from ref. 97.

($S = 1$). The corresponding wave-functions with maximum spin projection are the following:

$$\Psi_{gr}(S=0) = \tfrac{1}{\sqrt{2}}(|\varphi_A\bar{\varphi}_B| - |\bar{\varphi}_A\varphi_B|),$$
$$\Psi_{gr}(S=1, M_S=1) = |\varphi_A\varphi_B|, \quad (1)$$

When the electron transfer (that conserves the total spin value and its projection) is switched on, the ground manifold is split due to the mixing (interaction of configurations) with different CT states. The first kind of CT states (denoted as CT_1 in Fig. 1) arises from the virtual electron transfer from the single-occupied φ_A orbital of ion A to the single-occupied φ_B orbital of ion B and also from the back transfer $\varphi_B \rightarrow \varphi_A$ (the latter is not shown in Fig. 1). In accordance with Pauli's exclusion principle these CT states are spin singlets, and they are described by the wave-functions

$$\Psi^A_{CT_1} = |\varphi_A\bar{\varphi}_A|, \quad \Psi^B_{CT_1} = |\varphi_B\bar{\varphi}_B|. \quad (2)$$

The states CT_1 are separated from the ground manifold by a large (in comparison with the interatomic interaction) gap U which is the energy of the Coulomb repulsion between two electrons located at the same site and at the same orbital (intrasite repulsion) $\varphi_A(\varphi_B)$. These CT states are connected with the ground spin-singlet by the matrix elements

$$\langle\Psi^B_{CT_1}|\hat{V}(\varphi_A \rightarrow \varphi_B)|\Psi_{gr}(S=0)\rangle = \langle\Psi^A_{CT_1}|\hat{V}(\varphi_B \rightarrow \varphi_A)|\Psi_{gr}(S=0)\rangle = \sqrt{2}t_{\varphi\varphi}, \quad (3)$$

where $\hat{V}$ is the electron transfer operator, and $t_{\varphi\varphi} = \langle\varphi_B|\hat{h}|\varphi_A\rangle$ is the transfer integral connecting φ orbitals ($\varphi_A \leftrightarrow \phi_B$ electron hopping). The operator $\hat{V}$ can be associated with the one-electron Hamiltonian $\hat{h}$ for which the dominant contribution is provided by the kinetic energy of the delocalized electron. Note that only one of two microstates contributing to the ground spin-singlet state (namely, the microstate $|\uparrow\downarrow, M_S = 0\rangle$) is shown in Fig. 1. Using the second-order perturbation treatment one can find that the low lying spin-singlet $E(S = 0)$ is stabilized with respect to the spin-triplet due to the $t_{\varphi\varphi}$-transfer processes by the value

$$[E(S=1) - E(S=0)]_{\varphi_i \rightarrow \varphi_j} = 4t^2_{\varphi\varphi}/U. \quad (4)$$

We thus arrive at the important conclusion that the virtual electron transfer (Fig. 1) gives rise to the antiferromagnetic exchange contribution. Since the electronic jumps are induced by the kinetic energy of the electrons, this kind of the exchange is said to be "kinetic".

Another kind of the CT states can be obtained by the virtual electron transfer from a half-occupied φ orbital of one center to an empty orbital ϕ of another center (Fig. 2). This leads to the CT states with $S = 0$ (CT_2 state in Fig. 2) and $S = 1$ ($CT(S = 1)$ state in Fig. 2). Since the electron transfer matrix element is independent of the total spin-projection, only the spin-triplet states (ground and CT) with maximum spin-projection $M_S = 1$ are shown in Fig. 2. Note also that only one of two microstates is shown in Fig. 2 for both ground and CT_2 spin-singlet states. The gaps between the ground manifold and CT states CT_2 and $CT(S = 1)$ are equal to $U' + \Delta + K$ and $U' + \Delta - K$, respectively, where

$$K = \int\int \varphi_i(1)\phi_i(2)g(1,2)\phi_i(1)\varphi_i(2)d\tau_1 d\tau_2 \equiv \langle\varphi_i\phi_i|\hat{g}|\phi_i\varphi_i\rangle \quad (5)$$

is the intracenter exchange integral that is positive (*i.e.*, corresponds to the ferromagnetic intra-atomic exchange coupling that validates Hund's rule), and $\hat{g}$ is the inter-electronic repulsion, *i.e.*, two-electron part of the Hamiltonian. The effective energy includes also the gap Δ separating the orbital energies of each center. Finally, U' is the intrasite Coulomb repulsion between the electrons occupying different orbitals φ and ϕ (it is believed that $U' < U$). It can be seen that the spin-triplet state CT ($S = 1$) is lower in energy than the spin-singlet state CT_2 by the value $2K$ in accordance

with Hund's rule. The wave-functions for the states CT_2 and CT ($S = 1$) are given by

$$\Psi^{A}_{CT_2} = \tfrac{1}{\sqrt{2}}(|\varphi_A\bar{\phi}_A| - |\bar{\varphi}_A\phi_A|), \quad \Psi^{B}_{CT_2} = \tfrac{1}{\sqrt{2}}(|\varphi_B\bar{\phi}_B| - |\bar{\varphi}_B\phi_B|),$$
$$\Psi^{A}_{CT}(S = 1, M_S = 1) = |\varphi_A\phi_A|, \Psi^{B}_{CT}(S = 1, M_S = 1) = |\varphi_B\phi_B|, \quad (6)$$

where only the wave-functions with the maximum spin projection are shown for spin triplet CT states. The matrix elements connecting the spin-triplets prove to be the same as those connecting spin-singlets, namely

$$\begin{aligned}&\langle\Psi^{B}_{CT_2}|\hat{V}(\varphi_A \rightarrow \phi_B)|\Psi_{gr}(S = 0)\rangle \\ &= \langle\Psi^{A}_{CT_2}|\hat{V}(\varphi_B \rightarrow \phi_A)|\Psi_{gr}(S = 0)\rangle \\ &= \langle\Psi^{A}_{CT}(S = 1)|\hat{V}(\varphi_B \rightarrow \phi_A)|\Psi_{gr}(S = 1)\rangle \\ &= -\langle\Psi^{B}_{CT}(S = 1)|\hat{V}(\varphi_A \rightarrow \phi_B)|\Psi_{gr}(S = 0)\rangle = t_{\varphi\phi},\end{aligned} \quad (7)$$

where $t_{\varphi\phi} = \langle\phi_B|\hat{h}|\varphi_A\rangle = \langle\phi_A|\hat{h}|\varphi_B\rangle$ is the transfer parameter for the $\varphi_A \rightarrow \phi_B$ electron hopping. It is seen that the $t_{\varphi\phi}$ transfer stabilizes both the spin-singlet and the spin-triplet, but the stabilization of the spin-triplet is stronger due to the fact that it is closer in energy to the ground manifold. Applying again the second order perturbation procedure one finds that the $t_{\varphi\phi}$-transfer stabilizes the spin-triplet with respect to the spin-singlet by the value

$$\begin{aligned}&[E(S = 0) - E(S = 1)]_{\varphi\rightarrow\phi} \\ &= 2t^2_{\varphi\phi}\left(\frac{1}{U' + \Delta - K} - \frac{1}{U' + \Delta + K}\right) \approx 4t^2_{\varphi\phi}K/U^2.\end{aligned} \quad (8)$$

For the sake of simplicity in eqn (8) (and in Fig. 2) it is finally assumed that the gap Δ is small as compared to the Coulomb repulsion and $U \approx U'$. Such simplifying assumptions do not affect the qualitative results and will be used throughout this review. The interelectronic Coulomb repulsion of two electrons at the same center exceeds the intracenter exchange, and therefore in eqn (8) it is also assumed that $K/U \ll 1$. One can see that the energy of stabilization of the spin-triplet is smaller than that of the antiferromagnetic splitting that represents the third-order effect with respect to a small factor K/U. Finally, the overall exchange parameter includes both contributions, namely, antiferromagnetic related to the electron hopping between the half-filled orbitals and ferromagnetic arising from the transfer from the half-filled to the empty orbitals. For the reasons discussed thus far the first contribution usually dominates. In this context it is worth to mention the so-called Goodenough–Kanamori rules,[86] according to which the exchange coupling is antiferromagnetic if the electron transfer occurs between overlapping half-filled orbitals, and it is ferromagnetic if the electron virtually jumps from a half-filled to an empty orbital or alternatively, from a filled orbital to a half-filled one.

It is important to note that Anderson's mechanism of kinetic exchange demonstrated for a simple example of two one-electron centers can be extrapolated to a general case of the multielectron ions in polynuclear clusters that leads to the HDVV model. The magnetic and spectroscopic properties of a majority of known molecular magnets can be reproduced by the eigen-values of the isotropic spin HDVV Hamiltonian:

$$\hat{H}_{ex}(A,B) = -2J\hat{s}_A\hat{s}_B, \quad (9)$$

where $\hat{s}_A$ and $\hat{s}_B$ are the full spin operators of the many-electron metal centers. Here J is the multielectron exchange parameter which incorporates all pairwise virtual electron transfer pathways connecting half-filled orbitals of the coupled ions in their ground states. In general, along with the kinetic exchange the full multielectron exchange parameter includes also the contributions of the potential exchange. Such many-electron spin Hamiltonian constitutes the basis for the HDVV exchange model[1,14,15,84–86] which is widely used in molecular magnetism and solid state physics.

3. Restrictions of Heisenberg–Dirac–Van Vleck model

The HDVV model is rather general, but, at the same time, has a set of distinct restrictions that are to be especially emphasized in view of the main topic of this review. It should be stressed that the derivation of the HDVV Hamiltonian assumes interactions between orbitally non-degenerate ions, *i.e.* of ions in which the active orbital space of each center comprises only half-filled magnetic orbitals (as shown in Fig. 3, left part), and doubly occupied orbitals. Therefore the HDVV model is only applicable to systems comprising ions whose ground terms are orbitally non-degenerate and well isolated from the excited ones (*spin-clusters*). This is valid for the half-filled shells (t_2 and/or e) of transition metal ions in an octahedral crystal field, for example, high spin Fe^{III} ions with the ground term $^6A_{1g}(t^3_{2g}e^2_g)$, Cr^{III} ions with the half-filled t_2 shell giving rise to $^4A_{1g}(t^3_{2g})$ term, *etc.* In general, the ground term proves to be an orbital singlet for all transition metal ions in a strong low-symmetry crystal field that removes the orbital degeneracy and separates the ground state from the excited ones. If the low symmetry field is comparable with an effective energy of the exchange coupling the HDVV Hamiltonian also can not be applied and the exchange problem should be specially treated with due account for the pseudo-degeneracy.

Alternatively, when the orbital schemes include empty orbitals there are several electronic microstates with the same energy, which means that the corresponding crystal field term (multi-electron state) is orbitally degenerate as shown in the right side of Fig. 3 for different orbital configurations of the transition metal ions.

Such systems involving orbitally degenerate ions cannot be described by the HDVV model and for this reason they are referred to as non-Heisenberg systems. Fig. 4 shows electronic configurations of the d-ions in the octahedral crystal field (in conventional notations) with the indication on possible high spin (*h.s.*) and low-spin (*l.s.*) terms. Each scheme gives rise to a definite strong crystal field term although in general the terms are represented by the mixtures of different configurations (for instance, see discussion of the cobalt (II) problem in Section 4.2). From the scheme of electronic configurations one can conclude that only two electronic configurations, d^3 and d^5, give rise to orbital singlets in this symmetry.

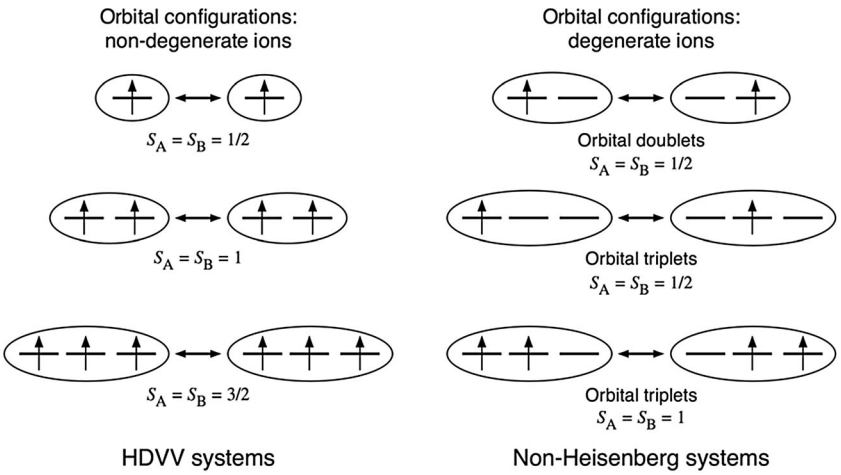

Fig. 3 Orbital schemes illustrating HDVV and non-Heisenberg systems. Adapted from ref. 97.

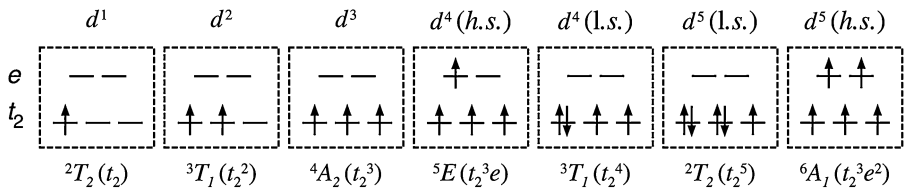

Fig. 4 Electronic configurations of the d-ions in octahedral crystal field.

4. Magnetic exchange in clusters containing orbitally-degenerate metal ions: concept of orbitally-dependent exchange and pseudo-spin-1/2 Hamiltonian

4.1 Orbitally-dependent exchange

Let us consider a special case of the degenerate system in which one of the constituent metal ions is orbitally degenerate and carries an orbital angular momentum while the second one is in an orbital singlet possessing a non-vanishing spin. This situation occurs in a simple system in which one ion (let say, A) possesses the ground term $^2T_{2g}(t_{2g}^1)$ (state with fictitious orbital angular momentum $l_A = 1$) in an ideal octahedral surrounding, whereas the ion B is located in an octahedral surrounding compressed along the tetragonal axis so that the orbital degeneracy is removed and the ground term of this ion is the orbital singlet $^2B_{2g}(b_{2g}^1)$. This situation can occur also in a heteroligand system in which an effective low-symmetry crystal field is induced by the ligand substitution. The entire system represents a corner shared dimer of D_{4h} symmetry and the tetragonal axis of the system coincides with the molecular A–B axis and with the local tetragonal axis along which the surrounding of the ion B is distorted (Fig. 5a). Thus, the exchange interaction should correspond to a $^2T_{2g}(t_{2g}^1) \otimes {}^2B_{2g}(b_{2g}^1)$ scheme (Fig. 5b).

It should be emphasized that Anderson's basic concept of kinetic exchange is applicable not only for the spin systems but also in the case of degeneracy (although the HDVV model is valid for the spin systems only). Thus, the kinetic exchange appears in the second order of perturbation theory due to the mixing of the states belonging to the ground manifold with the

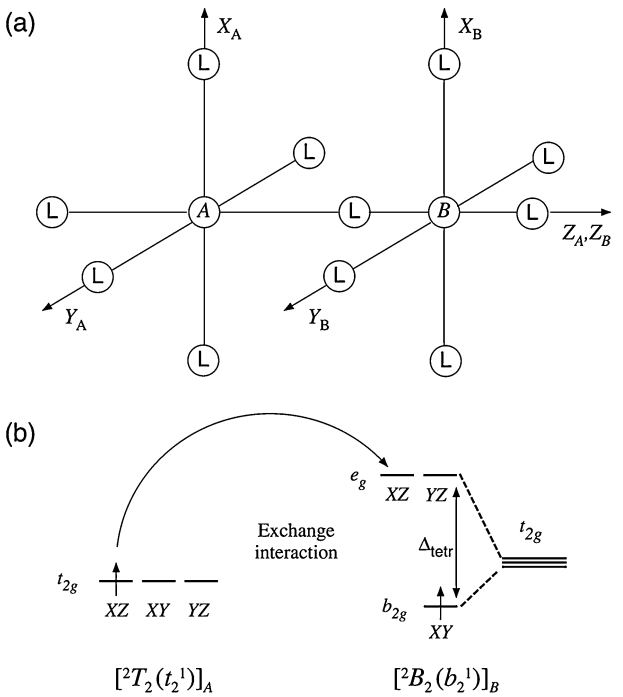

Fig. 5 The illustration for the $^2T_2(t_2^1) \otimes {}^2B_2(b_2^1)$-exchange problem: (a) topology of the system and coordinate axes; (b) tetragonal splitting for the site B and the scheme of the transfer processes in the kinetic exchange mechanism.

excited charge transfer (CT) states in which one electron is transferred from site A to site B. The one-electron t_{2g}-basis set for ion A is the following: $\xi \propto YZ, \eta \propto XZ, \zeta \propto XY$. For ion

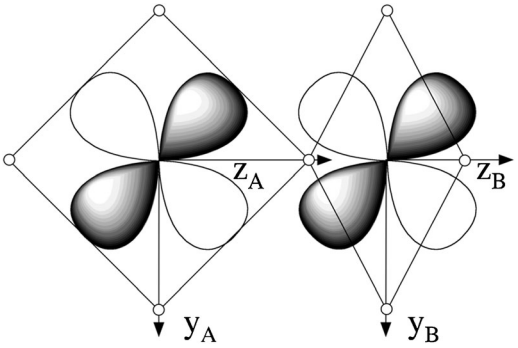

Fig. 6 Overlap scheme associated with the t_π-transfer.

B we have a b_{2g} orbital, $b_{2g} \propto XY$, and e-orbitals $\theta \propto YZ$, $\varepsilon \propto XZ$. In the case under consideration there are two kinds of one-electron transfer processes allowed by the overall tetragonal symmetry of the dimer. The first kind involves the processes $\xi_A \rightarrow \theta_B$ and $\eta_A \rightarrow \varepsilon_B$. These processes are associated with the π-overlap of the orbitals shown in Fig. 6 and are described by the hopping parameter $t_\pi = t(\xi,\theta) = t(\eta,\varepsilon)$. Another kind of transfer allowed by the symmetry is a δ-transfer that is described by the hopping parameter $t_\delta = t(\zeta,b_{2g})$. It is believed that $t_\pi \gg t_\delta$, so a relatively small δ-type contribution to the overall exchange can be neglected. The π-transfer processes contributing to the kinetic exchange are shown in Fig. 7a. The total spin of the dimer can take two values $S = 1$ and $S = 0$, so the ground manifold includes the spin-triplets and the spin-singlets. The spin-triplet states with the maximum spin projection $M_S = 1$ are expressed in terms of Slater determinants as follows:

$$\psi_\xi(S=1) = |\xi_A b_{2g}^B|,\ \psi_\eta(S=1) = |\eta_A b_{2g}^B|,\ \psi_\zeta(S=1) = |\zeta_A b_{2g}^B|. \quad (10)$$

Each spin-singlet is the superposition of two Slater determinants, for example:

$$\psi_\xi(S=0) = \tfrac{1}{\sqrt{2}}(|\xi_A \bar{b}_{2g}^B| - |\bar{\xi}_A b_{2g}^B|), \quad (11)$$

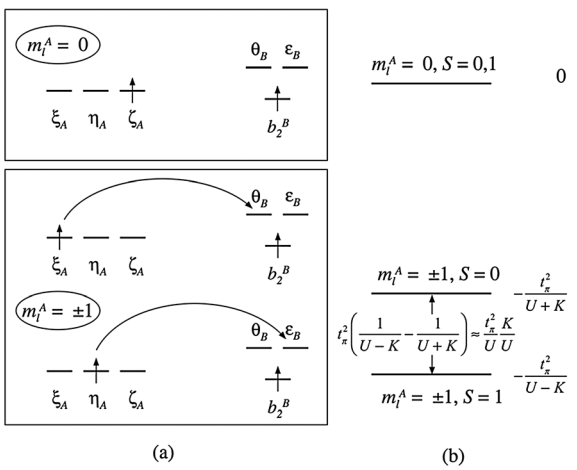

Fig. 7 Possible electron transfer processes (a) and energy pattern (b) for the $^2T_{2g}(t_{2g}^1) \otimes {}^2B_{2g}(b_{2g}^1)$-exchange problem. Only the first steps of the two-step processes are shown.

where ξ_A and $\bar{\xi}_A$ are the spin-orbitals with spin-up and spin-down, respectively.

The ground states $\psi_\zeta(S = 1)$ and $\psi_\zeta(S = 0)$ cannot be mixed with the CT states since the δ-transfer is neglected. For this reason the second-order corrections to the energies of these states are vanishing:

$$E_\zeta(S = 0) = E_\zeta(S = 1) = 0. \quad (12)$$

On the contrary, the states in which the orbitals ξ_A or η_A are occupied by one electron can be mixed with the CT states through the π-transfer processes. For example, the state $\psi_\xi(S = 1)$ is mixed with the CT spin-triplet $\psi_\theta(S = 1) = |b_{2g}^B \theta_B|$ separated from the ground state by the energy gap U–K, with U and K being the intraatomic Coulomb and exchange energies, respectively.[84,85] This mixing is defined by the electron transfer matrix element $\langle\psi_\xi(S = 1)|\hat{H}_{tr}|\psi_\theta(S = 1)\rangle = -t_\pi$ giving rise to the following second-order correction:

$$E_\xi(S=1) = -\frac{t_\pi^2}{U-K}. \quad (13)$$

The same expression can be found for the energy $E_\eta(S = 1)$. Similarly, the second-order corrections to the energies of spin-singlets are found to be

$$E_\xi(S=0) = E_\eta(S=0) = -\frac{t_\pi^2}{U+K}, \quad (14)$$

where $U + K$ is the energy gap between the ground state and the CT spin-singlets. Eqn (12)–(14) show that the exchange splittings of different states belonging to the ground manifold are different and depend on the occupation of the orbitals. For this reason, as distinguished from the HDVV exchange in spin-clusters, the exchange coupling involving orbitally-degenerate ions is *orbitally-dependent*.

The orbitally degenerate ions in crystal fields, in general, possess orbital magnetic moment which means that the matrix elements of the orbital angular momentum operators L_X, L_Y, L_Z have non-vanishing matrix elements within the crystal field wave-functions. Of course, these matrix elements (and corresponding mean values of the orbital magnetic contributions) are different from those for the free ions. It is conventional to use the so-called T–P isomorphism[87] that allows one to simplify calculations and to gain insight into the magnetic properties of metal ions. According to T–P isomorphism the cubic orbital triplet on site A can be regarded as the state with fictitious orbital angular momentum $l_A = 1$. This means that the 3 × 3 matrices of the orbital angular momentum operators within the three functions of the orbital triplet in a cubic field and those within the set of three atomic p-functions are different only by a common numerical factor. Then the functions of the dimer can be labeled as $|m_l^A;S,M_S\rangle$, where $S = 0,1$ is the total spin of the pair, and $m_l^A = 0,\pm1$ is the projection of the fictitious orbital angular momentum of the ion A. Note that the functions ξ_A and η_A are the linear combinations of the states with $m_l^A = \pm1$ while the function ζ_A represents the state with $m_l^A = 0$. Since the symmetry of the pair is axial (tetragonal), each energy level is characterized (along with the spin S) by $|m_l^A|$. Using this labeling, one can

present the energy levels of the exchange-coupled pair in the following form:

$$E(m_l^{\mathrm{A}} = 0;S) = 0,$$
$$E(|m_l^{\mathrm{A}}| = 1;S) = -\frac{t_\pi^2}{U+K} + \frac{1}{2}\left(\frac{t_\pi^2}{U+K} - \frac{t_\pi^2}{U-K}\right)S(S+1). \quad (15)$$

The entire energy pattern of the exchange splittings is essentially non-Heisenberg and does not follow Lande schemes (Fig. 7b). The ground multiplet with the energy $-t_\pi^2/(U-K)$ possesses $S = 1$ and $m_l^{\mathrm{A}} = \pm 1$. This $S = 1$ level is separated from the first excited $S = 0$ level by the gap $t_\pi^2\left(\frac{1}{U-K} - \frac{1}{U+K}\right) \approx \frac{t_\pi^2}{U}\frac{K}{U}$ and one can see that the orbitally-dependent kinetic exchange in this case produces a weak ferromagnetic effect. One can easily demonstrate that the energies in eqn (15) that have been obtained as a result of a direct calculation are the eigenvalues of the following exchange Hamiltonian:

$$\hat{H}_{\mathrm{ex}} = -\frac{1}{4}\left(\frac{3t_\pi^2}{U-K} + \frac{t_\pi^2}{U+K}\right)\hat{l}_{Z\mathrm{A}}^2 + \left(\frac{t_\pi^2}{U+K} - \frac{t_\pi^2}{U-K}\right)\hat{l}_{Z\mathrm{A}}^2\hat{\boldsymbol{s}}_{\mathrm{A}}\hat{\boldsymbol{s}}_{\mathrm{B}}, \quad (16)$$

where $\hat{l}_{Z\mathrm{A}}$ is the Z-component of the fictitious orbital angular momentum operator for the ion A. In fact using as a basis the states $|m_l^{\mathrm{A}},SM_S\rangle$ and taking into account that $\langle m_l^{\mathrm{A}}|\hat{l}_{Z\mathrm{A}}^2|m_l^{\mathrm{A}}\rangle = (m_l^{\mathrm{A}})^2$ and

$$\langle SM_S|\hat{\boldsymbol{s}}_{\mathrm{A}}\hat{\boldsymbol{s}}_{\mathrm{B}}|SM_S\rangle = \langle SM_S|\tfrac{1}{2}\left[(\hat{\boldsymbol{s}}_{\mathrm{A}}+\hat{\boldsymbol{s}}_{\mathrm{B}})^2 - \hat{\boldsymbol{s}}_{\mathrm{A}}^2 - \hat{\boldsymbol{s}}_{\mathrm{B}}^2\right]|SM_S\rangle = \tfrac{1}{2}[S(S+1) - \tfrac{3}{2}]$$

one easily arrives at the energies given by eqn (15). It is important to emphasize that this exchange Hamiltonian is drastically different from the HDVV spin-Hamiltonian and includes not only spin operators but also the orbital matrix $\hat{l}_Z^2$. The first term (term $\propto \hat{l}_{Z\mathrm{A}}^2$) is a pure *orbital part*, while the second-term (term $\propto \hat{l}_{Z\mathrm{A}}^2\hat{\boldsymbol{s}}_{\mathrm{A}}\hat{\boldsymbol{s}}_{\mathrm{B}}$) represents a *mixed spin-orbital part*. Such a complicated structure of the Hamiltonian is the main feature of the degenerate systems that distinguishes them from the exchange Hamiltonian for spin-clusters. In a general case, the orbitally-dependent Hamiltonian contains also the term $\propto \hat{\boldsymbol{s}}_{\mathrm{A}}\hat{\boldsymbol{s}}_{\mathrm{B}}$ which is of the same form as HDVV Hamiltonian. In this section the energy pattern has been directly calculated in a simple case on the basis of Anderson's model and then the concept of the orbitally-dependent exchange has been illustrated. The orbitally-dependent effective Hamiltonian (that, in fact, is a starting point for the theoretical treatment of degenerate systems) can be derived in its general form which means for all electronic configurations and crystal field terms by taking also into account for their mixing (see articles 88–96; for a full discussion see the review article 97).

Another important difference between the isotropic HDVV exchange and the orbitally-dependent exchange is that the latter is *strongly magnetically anisotropic*. In fact the analysis of the labeling of the energy levels in Fig. 7b shows that the orbitally-dependent exchange in the $^2T_{2g}(t_{2g}^1) \otimes {}^2B_{2g}(b_{2g}^1)$ pair produces a strong uniaxial magnetic anisotropy with the C_4 axis which proves to be the easy axis of the magnetization. Thus, in the presence of an external magnetic field directed along the C_4 axis the orbital part of Zeeman interaction $-\beta\kappa\hat{L}_Z H_Z$ splits the level $|m_l^{\mathrm{A}} \pm 1, S = 1\rangle$ into two Zeeman sublevels $|m_l^{\mathrm{A}} +1, S = 1\rangle$ and $|m_l^{\mathrm{A}} -1, S = 1\rangle$. In contrast, when the field is perpendicular to the C_4 axis, the orbital Zeeman interaction does not produce any splitting because all matrix elements of the operators $-\beta\kappa\hat{L}_X H_X$ and $-\beta\kappa\hat{L}_X H_X$ are vanishing within the $|m_l^{\mathrm{A}} = \pm 1, S = 1\rangle$ level. The same is true for the first excited level, although in this case $S = 0$ and therefore, only the orbital part of Zeeman interaction is operative. As far as the highest level is concerned, one observes that it is not split by the orbital Zeeman interaction in a parallel magnetic field, because this level has $m_l^{\mathrm{A}} = 0$. The main consequence of these features is that a strong magnetic anisotropy with $\chi_\parallel > \chi_\perp$ can be expected in the wide temperature range. We thus arrive at the conclusion that this case is somewhat similar to the classical case represented by an s–p-molecule (Van Vleck and Levi)[98–101] when the pair of ions is highly anisotropic due to the orbitally-dependent exchange in spite of the fact that the constituent ions are magnetically isotropic (as they are in ideal octahedral ligand surroundings).

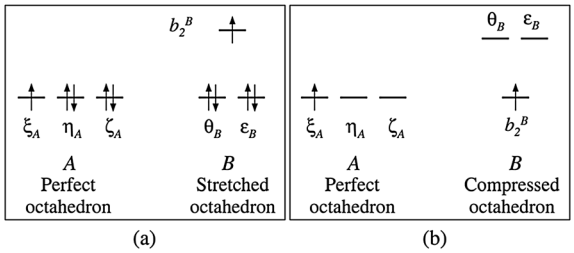

Fig. 8 Orbital schemes (selected microstates) for the dimer $^2T_{2g}(t_{2g}^5) \otimes {}^2B_{2g}(e_g^4b_{2g}^1)$ (a) and the complementary system $^2T_2(t_{2g}^1) \otimes {}^2B_2(b_{2g}^1)$ (b).

To complete the discussion of the orbitally-dependent exchange it should be mentioned that there is a remarkable equivalence of the exchange problems $^2T_{2g}(t_{2g}^5) \otimes {}^2B_{2g}(e_g^4b_{2g}^1)$ (Fig. 8a) and $^2T_{2g}(t_{2g}^1) \otimes {}^2B_{2g}(b_{2g}^1)$ (Fig. 8b) which can be attributed to the fact that the electron and the hole transfer processes contribute equally to the kinetic exchange. This is a general rule that is valid when one deals with the so-called complementary electronic configurations[87] of the exchange coupled metal ions.

4.2 Special cases of HDVV-like interactions between orbitally-degenerate ions

The analysis of different contributions to the kinetic exchange between the orbitally-degenerate metal ions shows that in some special (but at the same time rather important) cases this interaction proves to be orbitally-independent and isotropic and can be described by the Hamiltonian that has the same form, eqn (9), as the true HDVV Hamiltonian (we will term it *pseudo-Heisenberg Hamiltonian*).

In the first case the exchange splitting is assumed to mainly arise from electron transfer within orbitally-nondegenerate sub-shells of the orbitally-degenerate metal ions. The two notable examples of this situation are represented by the corner-shared pairs of octahedrally-coordinated high-spin Fe^{II} and Co^{II} ions with the overall symmetry D_{4h}. In these systems not only t_{2g} orbitals but also e_g orbitals,

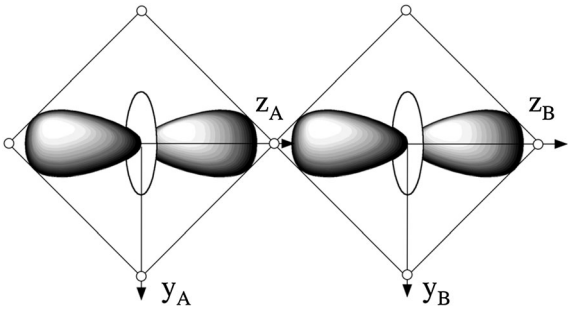

Fig. 9 Overlap scheme associated with the t_σ-transfer.

$u \propto 3Z^2-r^2$, $v \propto X^2-Y^2$, are occupied. The σ-transfer $u_A \leftrightarrow u_B$ shown in Fig. 9 is often the dominating process so that the π-transfer between weaker overlapping t_{2g}-orbitals seems to be less significant and can be neglected.

The ground cubic crystal field term of the high-spin Fe^{II} ion is $^5T_{2g}(t_{2g}^4e_g^2)$. It is notable that the σ-transfer occurs within the orbitally non-degenerate $e_g^2(^3A_{2g})$-subshells of the Fe^{II} ions (Fig. 10a). The exchange interaction between these subshells taken separately is obviously of the HDVV form. One can prove (and it is intuitively clear) that, in this case, the entire exchange splitting in the Fe^{II}–Fe^{II} pair can be described by the pseudo-Heisenberg exchange Hamiltonian with a good accuracy. The term "pseudo" reflects the fact that, as distinguished from the eigenvalues of the HDVV Hamiltonian, the energy levels are nine-fold orbitally degenerate and contain several multiplets.

Fig. 10b shows the σ-transfer process in a dimer composed of two high-spin Co^{II} ions. The wave-function of the ground state of Co^{II} ion represents a mixture of two $^4T_{1g}$ terms arising from two strong crystal field electronic configurations $t_{2g}^5e_g^2$ and $t_{2g}^4e_g^3$:

$$\Phi_{gr}(^4T_{1g}) = C_1|t_{2g}^5(^2T_{2g})e_g^2(^3A_{2g}), {}^4T_{1g}\rangle + C_2|t_{2g}^4(^3T_{1g})e_g^3(^2E_g), {}^4T_{1g}\rangle, \quad (17)$$

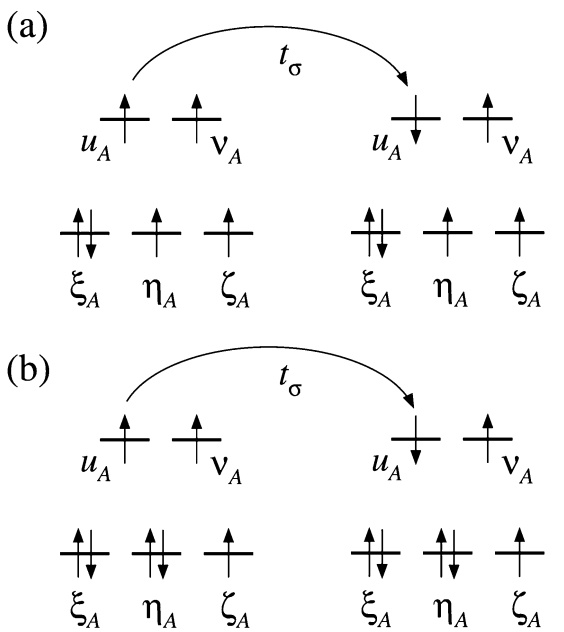

Fig. 10 Kinetic exchange mechanisms in Fe^{II}–Fe^{II} (a) and Co^{II}–Co^{II} (b) dimers.

where the coefficients are found by diagonalizing the matrix of the Coulomb mixing of two $^4T_{1g}$-terms.[87] One can find the following coefficients defining the degree of the mixture:

$$C_{1(2)} = \sqrt{(1^+_{(-)}w)/2}, \quad w = \frac{9B + 10Dq}{\sqrt{(9B + 10Dq)^2 + 144B^2}}. \quad (18)$$

Providing $Dq/B \ll 1$ (weak crystal field limit) one finds $C_1 = 2/\sqrt{5}$, $C_2 = 1/\sqrt{5}$ (^{4}F-state of the free Co^{II}-ion). In the strong field limit ($Dq/B \gg 1$) one obtains $C_1 = 1$, $C_2 = 0$.

Taking the values $B = 971\ cm^{-1}$ and $Dq = 840\ cm^{-1}$ for the Co^{II} complex with H_2O ligands[87] one obtains $C_1 \approx 0.956$, $C_2 \approx 0.294$. The second-order kinetic exchange corrections contain the squared matrix elements, so, in order to understand the relative importance of two $^4T_{1g}$ terms for the overall kinetic exchange splittings, one has to compare the squares of the coefficients C_1 and C_2 that can be estimated as: $C_1^2 \approx 0.914$, $C_2^2 \approx 0.086$. One thus arrives at the conclusion that the contribution of the $^4T_{1g}(t_{2g}^4e_g^3)$ term to the kinetic exchange splittings is small as compared with that of the $^4T_{1g}(t_{2g}^5e_g^2)$ term. Therefore the exchange interaction between two high-spin Co^{II} ions can be described with a high accuracy by considering the $^4T_{1g}(t_{2g}^5e_g^2) \otimes {}^4T_{1g}(t_{2g}^5e_g^2)$-exchange as schematically shown in Fig. 10b. Assuming $t_\sigma \gg t_\pi$ we thus obtain that the Co^{II}–Co^{II} exchange interaction is related to the electron transfer between the orbitally nondegenerate $e_g^2(^3A_{2g})$-subshells and can approximately be described by the pseudo-Heisenberg Hamiltonian. This statement forms the background of the so-named Lines model[102,103] that is widely used in magnetochemistry and spectroscopy of exchange coupled Co^{II} compounds.[104–106] In the framework of this model the first-order orbital angular momentum of each high-spin Co^{II} ion is taken into account by considering the SO coupling and (if necessary) the low-symmetry crystal field which distorts the octahedral ligand surroundings of the Co^{II} ion, whereas the exchange interaction between the Co^{II} ions is taken in the HDVV form. An interesting example of the system for which the Lines model proves to be a good approximation is provided by the heterotrimetallic complex $[Co_2PdCl_2(dpa)_4]$ in which two magnetic Co^{II} ions are separated by the non-magnetic Pd^{II} ion.[107] Due to the large spatial extension of 4d-orbitals the $3d_{Z^2}$-orbitals of the Co^{II} ions strongly overlap through the $4d_{Z^2}$ orbital of the Pd^{II} ion giving rise to the strong σ-transfer between the orbitally-nondegenerate electronic subshells and thus to the pseudo-Heisenberg exchange Hamiltonian. Due to the importance of the orbital magnetic contribution and related magnetic anisotropy, the study of dinuclear and polynuclear cobalt(II) compounds became a special area of molecular magnetism (summarized in the recent review article 108). This area is closely related to single molecular magnetism and holds promise for the important trends such as the design of new SMMs in a controllable way and low temperature magnetic refrigerants which can replace helium-3.[109]

The second important case can be illustrated by considering the magnetic exchange in a corner-shared d^1–d^1 dimer of D_{4h} symmetry in which the octahedral ligand environment of the ion A is strongly stretched along the tetragonal axis of the dimer, while the octahedral environment of the ion B is

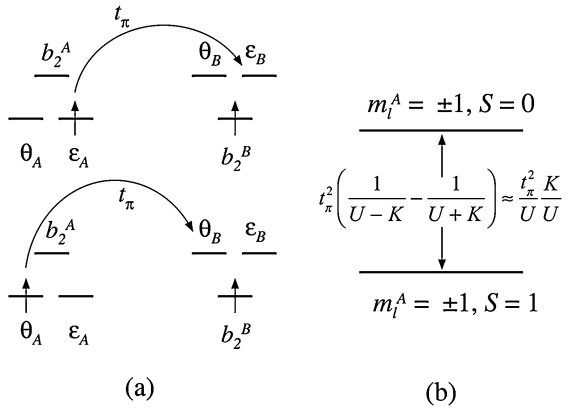

Fig. 11 Electron transfer processes (a) and energy pattern (b) for the $^2E_g(e_g^1) \otimes {}^2B_{2g}(b_{2g}^1)$-exchange problem.

compressed along this axis. In this case the $^2T_{2g}(t_{2g}^1)$ cubic term is split in such a way that the ground term of the ion A is the orbital doublet $^2E_g(e_g^1)$, while the ground term of the ion B is the orbital singlet $^2B_{2g}(b_{2g}^1)$ so we deal with the $^2E_g(e_g^1) \otimes {}^2B_{2g}(b_{2g}^1)$ exchange problem. Only the π-transfer is taken into account as depicted in Fig. 11a. The functions θ_A and ε_A are the linear combinations of the states with the fictitious orbital angular momentum projections $m_l^A = \pm 1$. Evaluation of the energy levels leads to the energy pattern shown in Fig. 11b, from which one can observe a weak ferromagnetic exchange splitting of the order of $(t_\pi^2/U)(K/U)$:

$$E(M_L = \pm 1; S) = -\frac{t_\pi^2}{U+K} + \frac{1}{2}\left(\frac{t_\pi^2}{U+K} - \frac{t_\pi^2}{U-K}\right)S(S+1). \tag{19}$$

These energies are the eigenvalues of the exchange Hamiltonian

$$\hat{H}_{ex} = -\frac{1}{4}\left(\frac{t_\pi^2}{U+K} + \frac{3t_\pi^2}{U-K}\right) + \left(\frac{t_\pi^2}{U+K} - \frac{t_\pi^2}{U-K}\right)\hat{\boldsymbol{s}}_A\hat{\boldsymbol{s}}_B, \tag{20}$$

which formally coincides with the HDVV Hamiltonian, eqn (9), if one omits the spin-independent term in eqn (20) and sets

$$J = \frac{1}{2}\left(\frac{t_\pi^2}{U-K} - \frac{t_\pi^2}{U+K}\right). \tag{21}$$

It is to be noted, however, that the energy pattern cannot be referred to as a true HDVV scheme due to presence of the non-vanishing orbital magnetic contribution. One can see that, as distinguished from the spin clusters, the system under consideration exhibits strong uniaxial magnetic anisotropy with the tetragonal axis being an easy axis of the magnetization. At the same time this anisotropy is associated with the single-ion anisotropy of the orbitally-degenerate ion A but not with the exchange interaction which is isotopic and *orbitally-independent* (*pseudo-Heisenberg*) in the case under consideration. This statement seems to be valid for all situations when the number of equal hopping parameters contributing to the kinetic exchange is equal to the total orbital multiplicity of the system. In fact, here we have two equal hopping parameters $t_{\theta\theta} = t_{\varepsilon\varepsilon} \equiv t_\pi$ and the total orbital multiplicity is also equal to two.

4.3 The case of strong spin–orbit coupling: pseudo-spin-1/2 Hamiltonian

In Sections 4.1 and 4.2 we focused solely on the exchange interaction and omitted the role of the spin–orbit (SO) coupling in the discussion which is inherent to the problem of the orbital degeneracy. To illustrate the effect of SO coupling let us turn back to the case of the $^2T_{2g}(t_{2g}^5) \otimes {}^2B_{2g}(e_g^4b_{2g}^1)$ exchange coupled pair shown in Fig. 8a. The effective SO coupling Hamiltonian acting within the $^2T_{2g}(t_{2g}^5)$ term of the ion A is presented as:[5]

$$\hat{H}_{SO} = -\kappa\lambda\,\hat{\boldsymbol{l}}_A\hat{\boldsymbol{s}}_A, \tag{22}$$

where $\hat{\boldsymbol{l}}_A$ is the operator of the fictious orbital angular momentum of the ion A, κ is the orbital reduction factor and λ is the SO coupling parameter that is negative for the case under consideration (more than half-filled t_2-shell). The minus sign in eqn (22) appears due to the fact that the matrices of the orbital angular momentum defined in the cubic T_{2g} basis and the free atomic p-basis differ in sign.[87] The SO coupling splits the $^2T_{2g}$-term (state with $l_A = 1$, $m_l^A = 0, \pm 1$) into the Kramers doublet Γ_7 (state with the total angular momentum $j_A = 1/2$) and the quadruplet Γ_8 ($j_A = 3/2$), with the ground state being the Kramers doublet (Fig. 12). In many cases the energy gap $\frac{3}{2}\kappa|\lambda|$ between the states Γ_7 and Γ_8 significantly exceeds the exchange splitting. At low temperatures when only the ground Kramers doublet is significantly populated, we arrive at the widely used effective pseudo-spin-1/2 Hamiltonian approach[110–121] in which the excited spin-orbital multiplets are neglected and only the ground Kramers doublet is taken into account. Within this formalism the initial $^2T_{2g}(t_{2g}^5) \otimes {}^2B_{2g}(e_g^4b_{2g}^1)$ exchange problem is reduced to the $\Gamma_7(t_{2g}^5) \otimes {}^2B_2(e_g^4b_{2g}^1)$ problem in which a ground Kramers doublet (pseudo-spin-1/2) of the ion A is coupled with a true spin 1/2 of the ion B as illustrated in Fig. 12.

The ground Kramers doublet level for the ion A can be built by means of the Clebsch–Gordan coupling scheme in which two angular momenta $l_A = 1$ and $s_A = 1/2$ are coupled to give states with the total angular momenta $j_A = 3/2$ and $j_A = 1/2$. Then, the wave functions $|j_A m_j^A\rangle$ are expressed in terms of the uncoupled basis $|l_A m_l^A, s_A m_s^A\rangle \equiv |m_l^A, m_s^A\rangle$ as follows:

$$|j_A = 1/2,\ \ m_j^A = \pm 1/2\rangle, = \sum_{m_l^A, m_s^A} C^{1/2,m_j^A}_{1\,m_l^A,1/2\,m_s^A}|m_l^A, m_s^A\rangle, \tag{23}$$

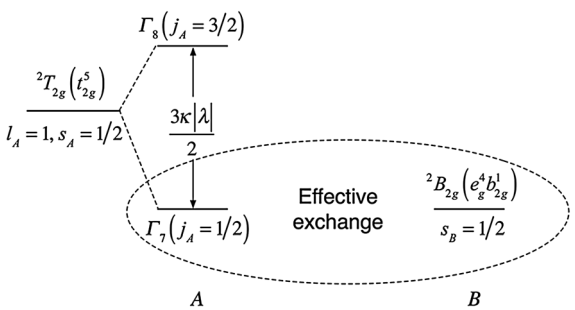

Fig. 12 Effective pseudo-spin-1/2 interaction in the $\Gamma_7(t_{2g}^5) \otimes {}^2B_2(e_g^4b_{2g}^1)$-pair.

where $C^{1/2,m_j^A}_{1\,m_l^A,1/2\,m_s^A}$ are the Clebsch–Gordan coefficients[122] and the summation runs over all quantum numbers m_l^A,m_s^A. Application of this procedure gives the following result:

$$|\tfrac{1}{2}\tfrac{1}{2}\rangle = \sqrt{\tfrac{2}{3}}|1,-\tfrac{1}{2}\rangle - \tfrac{1}{\sqrt{3}}|0,\tfrac{1}{2}\rangle,$$
$$|\tfrac{1}{2}-\tfrac{1}{2}\rangle = -\sqrt{\tfrac{2}{3}}|-1,\tfrac{1}{2}\rangle + \tfrac{1}{\sqrt{3}}|0,-\tfrac{1}{2}\rangle. \quad (24)$$

At this point we need to establish the correspondence between these states and the pseudo-spin-1/2 states $|\tau_A = \frac{1}{2}, \sigma_A = \pm\frac{1}{2}\rangle$, where $\tau_A = \frac{1}{2}$ and $\sigma_A = \pm\frac{1}{2}$ are the quantum numbers of the pseudo-spin and its projection, respectively. Let us define the effective Zeeman Hamiltonian for the ion A. This Hamiltonian acts within the Kramers doublet space and has the form

$$\hat{H}_Z^{\text{eff}}(A) = \beta g_{\text{eff}} \hat{\boldsymbol{\tau}}_A \boldsymbol{H}, \quad (25)$$

where g_{eff} is the effective g-factor for the Kramers doublet and $\boldsymbol{H}$ is the magnetic field. Comparing the matrix of the initial Zeeman Hamiltonian $\beta(g_e\hat{\boldsymbol{s}}_A - \kappa\hat{\boldsymbol{l}}_A)\boldsymbol{H}$ with that of $\hat{H}_Z^{\text{eff}}$ and demanding g_{eff} to be positive we arrive at the conclusion that this requirement can be fulfilled only if $|\tau_A = \frac{1}{2}, \sigma_A = \frac{1}{2}\rangle$ corresponds to $|j_A = 1/2, m_j^A = -1/2\rangle$ and $|\tau_A = \frac{1}{2}, \sigma_A = \frac{1}{2}\rangle$ corresponds to $|j_A = -1/2, m_j^A = 1/2\rangle$. For this correspondence one finds:

$$g_{\text{eff}} = \tfrac{1}{3}(g_e + 4\kappa). \quad (26)$$

Let us calculate the matrix of the orbitally-dependent exchange Hamiltonian, eqn (8), within the truncated basis of the Kramers doublet, eqn (24). Simple calculations show that within this basis the matrix $\hat{l}^2_{ZA}$ coincides with the $\frac{2}{3}\hat{I}_A$ matrix, where $\hat{I}_A$ is the unit matrix. We also find that the matrix $\hat{l}^2_{ZA}\hat{s}_{Z_A}$ coincides with the $\frac{2}{3}\hat{\tau}_Z^A$ matrix, where $\hat{\tau}_Z^A$ is the Z component of the pseudo-spin-1/2 matrix

$$\hat{\tau}_Z^A = \begin{pmatrix} 1/2 & 0 \\ 0 & -1/2 \end{pmatrix} \quad (27)$$

defined in the basis $|\tau_A = \frac{1}{2}, \sigma_A = \frac{1}{2}\rangle$, $|\tau_A = \frac{1}{2}, \sigma_A = -\frac{1}{2}\rangle$. Finally we obtain the result that all matrix elements of the operators $\hat{l}^2_{ZA}\hat{s}_{X_A}$ and $\hat{l}^2_{ZA}\hat{s}_{Y_A}$ are vanishing within the Kramers doublet space. So, upon the projection on the ground manifold $\Gamma_7(t_{2g}^5) \otimes {}^2B_{2g}(e_g^4 b_{2g}^1)$ the initial exchange Hamiltonian, eqn (16), is reduced to the pseudo-spin-1/2 Hamiltonian having an Ising form

$$\hat{H}_{\text{ex}}^{\text{eff}} = -2J_\parallel \hat{\tau}_Z^A \hat{s}_Z^B, \quad (28)$$

where the effective exchange parameter takes the following form:

$$J_\parallel = \frac{1}{3}\left(\frac{t_\pi^2}{U-K} - \frac{t_\pi^2}{U+K}\right). \quad (29)$$

In eqn (28) the term proportional to the unit matrix is omitted. It follows from eqn (28) that $J_\parallel > 0$, so the exchange interaction in this case is ferromagnetic in compliance with the Goodenough–Kanamori rules.[86] In fact, the π-type electron transfer occurs from the doubly occupied orbital of the ion B to the single-occupied orbital of the ion A (Section 4.1) and in accord with the Goodenough–Kanamori rules, such a kind of transfer produces a ferromagnetic exchange splitting.

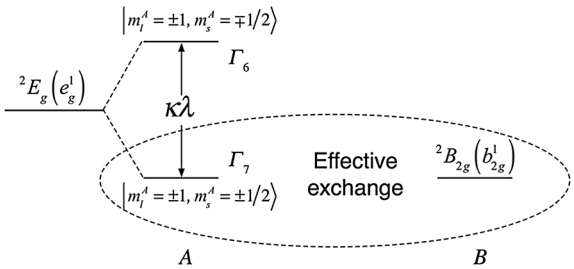

Fig. 13 Effective pseudo-spin-1/2 interaction in the $\Gamma_7(e_g^1) \otimes {}^2B_{2g}(b_{2g}^1)$-pair.

Finally, it should be emphasized that in the present case the strong uniaxial Ising type anisotropy is a direct consequence of the orbitally-dependent exchange because both constituent metal ions are fully isotropic (no single-ion anisotropy exists).

As other example illustrating the idea of the pseudo-spin-1/2 Hamiltonian approach we will reconsider now the aforenamed case of the $^2E_g(e_g^1) \otimes {}^2B_{2g}(b_{2g}^1)$-problem (Section 4.2) taking into account the SO splitting of the tetragonal $^2E_g(e_g^1)$-term. Since the basis functions for the E_g-term on the center A correspond to $m_l^A = \pm1$ the transverse part $-\kappa\lambda(\hat{l}_{X_A}\hat{s}_{X_A} + \hat{l}_{Y_A}\hat{s}_{Y_A})$ of the SO coupling operator is not operative within the ^2E_g-term. For this reason the effective SO coupling operator is reduced to the axial form:

$$\hat{H}_{\text{SO}}(^2E_g) = -\kappa\lambda\hat{l}_{ZA}\hat{s}_{Z_A}, \quad (30)$$

where the SO coupling parameter λ is positive (less than half-filled e_g-shell). This interaction splits the ^2E_g-term into two Kramers doublets $\Gamma_7(m_l^A = \pm1, m_s^A = \pm\frac{1}{2})$ and $\Gamma_6(m_l^A = \pm1, m_s^A = \mp\frac{1}{2})$ with the Γ_7 state being the ground one and the levels Γ_7 and Γ_6 being separated by the gap $\kappa\lambda$ (Fig. 13). When this gap significantly exceeds the exchange splitting and the temperature is too low to populate the excited Kramers doublet, one arrives at the pseudo-spin-1/2 Hamiltonian formalism in which the initial $^2E_g(e_g^1) \otimes {}^2B_{2g}(b_{2g}^1)$ exchange problem is reduced to the $\Gamma_7(e_g^1) \otimes {}^2B_{2g}(b_{2g}^1)$ problem (Fig. 13), and the Kramers doublet Γ_7 is regarded as a pseudo-spin-1/2 state.

In order to establish the correspondence between the wave-functions $|m_l^A = \pm1, m_s^A = \pm\frac{1}{2}\rangle$ and the components $|\sigma_A = \pm\frac{1}{2}\rangle$ of the pseudo-spin-1/2 we will introduce the effective Zeeman operator for the Kramers doublet ion A and calculate the principal values of the effective g-tensor. Due to the tetragonal symmetry on the center A this operator has the form

$$\hat{H}_Z^{\text{eff}}(A) = \beta[g_\parallel \hat{\tau}_Z^A H_Z + g_\perp(\hat{\tau}_X^A H_X + \hat{\tau}_Y^A H_Y)], \quad (31)$$

where $g_\parallel$ and $g_\perp$ are the principal values of the local effective g-tensor of the center A. To find the principal values of the effective g-tensor one has to compare the matrix elements of this operator with the matrix of the initial Zeeman operator $\hat{H}_z(A) = \beta(g_e\hat{\boldsymbol{s}}_A - \kappa\hat{\boldsymbol{l}}_A)\boldsymbol{H}$ acting within the basis $|m_l^A = \pm1, m_s^A = \pm1/2\rangle$. All matrix elements of the operators $\hat{\boldsymbol{s}}_X^A$, $\hat{\boldsymbol{s}}_Y^A$, $\hat{l}_X^A$ and $\hat{l}_Y^A$ vanish within this basis, so one immediately finds that $g_\perp = 0$. On the other hand by setting $g_e = 2$ one can find

$$\langle m_l^A = \pm1, m_s^A = \pm1/2|\beta(2\hat{s}_Z^A - \kappa\hat{l}_Z^A)$$
$$H_z|m_l^A = \pm1, m_s^A = \pm1/2\rangle = \pm\beta(1-\kappa)H_z, \quad (32)$$

Since $\langle\sigma_A = \pm1/2|\hat{H}_Z^{eff}(A)|\sigma_A = \pm1/2\rangle = \pm\frac{1}{2}\beta g_{\|}H_z$, $g_{\|} = 2(1-\kappa)$ is positive (note that $\kappa < 1$) provided that the state $|m_l^A = 1, m_s^A = \frac{1}{2}\rangle$ corresponds to $|\sigma_A = \frac{1}{2}\rangle$ and the state $|m_l^A = -1, m_s^A = -\frac{1}{2}\rangle$ to $|\sigma_A = -\frac{1}{2}\rangle$. Since the orbital reduction factor is close to 1, the value $g_{\|}$ is small due to mutual canceling of the orbital and spin contributions, so we come to the conclusion that the ion A is weakly magnetic at low temperatures.

Let us evaluate now the matrix of the pseudo-Heisenberg exchange Hamiltonian, eqn (12), within the $|m_l^A = \pm1, m_s^A = \pm\frac{1}{2}\rangle$ basis. It is seen that

$$\langle m_l^A = \pm1, m_s^A = \pm\tfrac{1}{2}|\hat{s}_{Z_A}|m_l^A = \pm1, m_s^A = \pm\tfrac{1}{2}\rangle = \pm\tfrac{1}{2}, \quad (33)$$

while all matrix elements of the operators $\hat{\boldsymbol{s}}_{XA}$ and $\hat{\boldsymbol{s}}_{YA}$ are vanishing within this basis. Then projecting the initial exchange Hamiltonian, eqn (20), on the $\Gamma_7(e_g^1) \otimes {}^2B_{2g}(b_{2g}^1)$ manifold and omitting the term proportional to the unit matrix we obtain the pseudo-spin-1/2 Hamiltonian of the Ising form in which the $J_{\|}$ parameter is given by

$$J_{\|} = \frac{1}{2}\left(\frac{t_\pi^2}{U-K} - \frac{t_\pi^2}{U+K}\right). \quad (34)$$

The effective exchange proves to be ferromagnetic ($J_{\|} > 0$) in accordance with the Goodenough–Kanamori rules[86] since the π-type electron transfer in this case occurs from the single occupied orbital of the ion A to the empty orbital of the ion B (Section 4.2).

The obtained result can be regarded as a part of a more common rule according to which, if the initial exchange interaction involving the axially anisotropic metal ions (for example those with the ground tetragonal *E*-terms) is of the isotropic pseudo-Heisenberg form, the effective pseudo-spin-1/2 Hamiltonian for the ground Kramers doublets takes on the fully anisotropic Ising form. Note, that as distinguished from the previous example, this anisotropy cannot be regarded as exchange anisotropy since the exchange itself is fully isotropic in accordance with eqn (20). Indeed, in spite of the fact that it appears as anisotropy of the effective pseudo-spin-1/2 exchange, such anisotropy is to be related to the single-ion rather than to the exchange.

Finally, let us briefly discuss the case when the exchange interaction between isotropic orbitally-degenerate ions is described by the pseudo-Heisenberg Hamiltonian $\hat{H}_{ex} = -2J\hat{\boldsymbol{s}}_A\hat{\boldsymbol{s}}_B$ in which $\hat{\boldsymbol{s}}_A$ and $\hat{\boldsymbol{s}}_B$ are the true spin operators. This is, for instance, the case of two octahedrally coordinated high-spin Co^{II} ions provided that the dominating electron transfer links the orbitally nondegenerate $e_g^2({}^3A_{2g})$-subshells of two cobalt ions. The ${}^4T_{1g}$ term of *i*-th Co^{II} ion (i = A, B) can be regarded as the state with fictitious angular momentum $l_i = 1$. This orbital angular momentum is coupled with the true spin $s_i = 3/2$ by the SO coupling:

$$\hat{H}_{SO}^i = -(3/2)\kappa\lambda\hat{\boldsymbol{l}}_i\hat{\boldsymbol{s}}_i, \quad (35)$$

where $\lambda \approx -180$ cm^{-1} [5] is the SO coupling parameter for the Co^{II} ion. The SO coupling splits the ground ${}^4T_{1g}$ term into the following states characterized by the total angular momentum j_i: ground Kramers doublet $j_i = 1/2(\Gamma_6)$, quartet $j_i = 3/2(\Gamma_8)$ and sextet $j_i = 5/2(\Gamma_7 + \Gamma_8)$ with the energies $(15/4)\kappa\lambda$, $(3/2)\kappa\lambda$ and $-(9/4)\kappa\lambda$, respectively. Applying the above described procedure one finds the following interrelationship between the operator $\hat{\boldsymbol{s}}_i$ defined in the Kramers-doublet basis and the spin-1/2 operator $\hat{\boldsymbol{\tau}}_i$:[102]

$$\hat{\boldsymbol{s}}_i = (5/3)\hat{\boldsymbol{\tau}}_i. \quad (36)$$

Then projecting the initial pseudo-Heisenberg Hamiltonian $\hat{H}_{ex} = -2J\hat{\boldsymbol{s}}_A\hat{\boldsymbol{s}}_B$ onto the ground $\Gamma_6(t_{2g}^5e_g^2) \otimes \Gamma_6(t_{2g}^5e_g^2)$ manifold we arrive at the following pseudo-spin-1/2 Hamiltonian:

$$\hat{H}_{ex}^{eff} = -(50/9)J\hat{\boldsymbol{\tau}}_A\hat{\boldsymbol{\tau}}_B. \quad (37)$$

The Hamiltonian, eqn (37), is of the HDVV form and fully isotropic in accordance with the fact that in this case both single-ion and exchange anisotropic contributions are vanishing.

5. Applications of the concepts of the orbitally-dependent exchange and pseudospin-1/2 Hamiltonian

5.1 Orbitally-dependent exchange and magnetic anisotropy in $[Ti_2Cl_9]^{3-}$

In this section we will consider the properties of some molecular systems exhibiting orbital degeneracy and show how the unquenched orbital angular momentum manifests itself in their properties. In some cases we will use the model examples so far discussed and show how the simple models can work to give a qualitative picture in more complex situations.

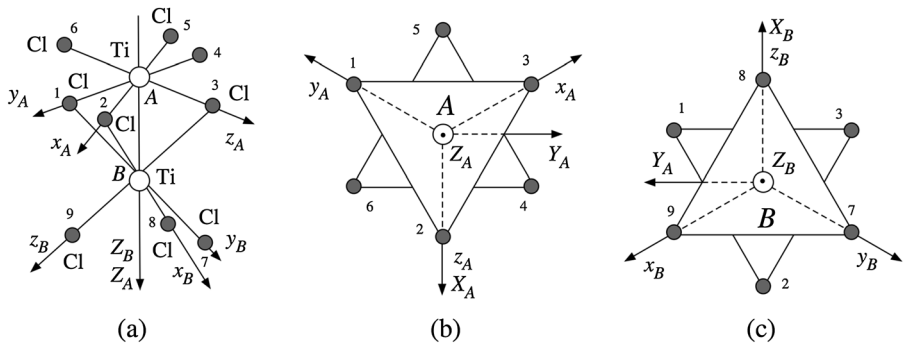

Fig. 14 Molecular structure of the $[Ti_2Cl_9]^{3-}$ unit. Cartesian cubic and trigonal frames for a face-shared binuclear system: local cubic frames (a), local trigonal frames for the sites A (b) and B (c). Adapted from ref. 92.

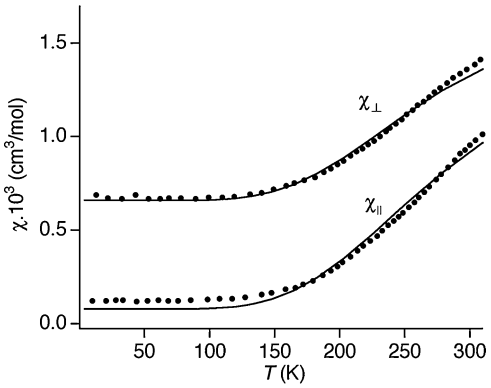

Fig. 15 Comparison between the experimental $\chi_{\parallel}$ *vs.* T and $\chi_{\perp}$ *vs.* T curves measured for the $[Ti_2Cl_9]^{3-}$ unit (dots)[126] and the theoretical curves (solid lines)[92] calculated with $A = 141\,000\ cm^{-1}$, $B = 900\ cm^{-1}$, $C = 3300\ cm^{-1}$, $\lambda = 155\ cm^{-1}$, $t_a = -5208\ cm^{-1}$, $t_e = -0.154t_a$, $\Delta_{trig} = 320\ cm^{-1}$, and $\kappa = 0.71$. Adapted from ref. 92.

The Ti^{III} ions are located in well isolated face-shared dimers of D_{3h} symmetry (Fig. 14) in the crystal structure of $Cs_3Ti_2Cl_9$ and $Cs_3Ti_2Br_9$ (see ref. 5 and refs. therein). The magnetic and spectroscopic properties of these systems were debated for almost two decades.[92,123–125] The ground cubic term of the Ti^{III} ion is $^2T_{2g}(t_{2g}^1)$, so, in the case of perfect octahedral ligand surroundings of the Ti^{III} ions, we face a $^2T_{2g}(t_{2g}^1) \otimes {}^2T_{2g}(t_{2g}^1)$ exchange problem in a pair of D_{3h} symmetry.

The temperature dependence of $\chi_{\parallel}$ and $\chi_{\perp}$ measured in ref. 126 (Fig. 15) indicates that the low-temperature magnetic susceptibility is small and strongly anisotropic with $\chi_{\perp} > \chi_{\parallel}$. This significant magnetic anisotropy indicates the importance of the orbital interactions. A remarkable feature of the experimental data is that the magnetic anisotropy decreases with the increase of temperature. Both $\chi_{\parallel}$ and $\chi_{\perp}$ decrease when the samples cool down and they become temperature independent at $T < 100$ K. These data clearly indicate that the ground state of the pair is non-magnetic.

The idealized molecular structure of $[Ti_2Cl_9]^{3-}$ and the local coordinate frames associated with the metal sites are shown in Fig. 14. It is convenient to introduce the trigonal local coordinates X_A,Y_A,Z_A and X_B,Y_B,Z_B with $Z_A(Z_B)$ axes directed along the C_3 axis. In Fig. 14 these frames are shown together with the cubic ones (x_A,y_A,z_A and x_B,y_B,z_B). The molecular frame is chosen to coincide with the local trigonal frame X_A,Y_A,Z_A. The real trigonal forms of t_2 orbitals on each metal center are defined by

$$\begin{aligned} a_2 &= d_{Z^2}, \\ \theta_2 &= (1\sqrt{3})(-d_{XZ} + \sqrt{2}d_{X^2-Y^2}), \\ \varepsilon_2 &= (1\sqrt{3})(-d_{YZ} - \sqrt{2}d_{XY}). \end{aligned} \qquad (38)$$

These orbitals refer to the local trigonal X_i,Y_i,Z_i (i = A,B) frames; the index i is omitted in eqn (38). It should be emphasized that the $TiCl_6$ octahedra are slightly distorted along the trigonal axis resulting in the splitting of the ground $^2T_{2g}$ term of the Ti^{III} ion into the orbital singlet $^2A_1$ and the orbital doublet ^2E, with the orbital singlet $^2A_1$ being the ground term. We will denote the energy gap $^2A_1 - {}^2E$ due to the local trigonal crystal field as Δ_{trig}. As a result of the lowering of the site symmetry from O to C_{3v}, the a_2-orbital becomes the a_1-type orbital while the orbitals θ_2 and ε_2 prove to be the e-type orbitals. While considering the kinetic exchange in $[Ti_2Cl_9]^{3-}$ one should take into account that in trigonal symmetry there are the following two non-vanishing transfer integrals:

$$t(a_2^A,a_2^B) \equiv t_a\ (a_1\text{–}a_1\text{—transfer process}), \qquad (39)$$

$$t(\theta_2^A,\theta_2^B) = t(\varepsilon_2^A,\varepsilon_2^B) \equiv t_e\ (e\text{–}e\text{—transfer process}).$$

The trigonal crystal field splits the ground manifold $^2T_{2g}(t_{2g}^1) \otimes {}^2T_{2g}(t_{2g}^1)$ into the following groups of states: (i) the lowest in energy group $(^2A_1)_A \otimes (^2A_1)_B$ (abbreviated as a $\otimes$ a-group) that appears as a result of the exchange splitting of the ground multiplet of two non-interacting Ti^{III} ions; (ii) the first excited group $(^2A_1)_A \otimes (^2E)_B$, $(^2E)_A \otimes (^2A_1)_B$ (a $\otimes$ e-group) that arises from the multiplet with the energy Δ_{trig}; and (iii) the highest in energy group of states $(^2E)_A \otimes (^2E)_B$ (e $\otimes$ e-group) arising from the multiplet with the energy $2\Delta_{trig}$. Along with the kinetic exchange and the trigonal crystal field term, the full Hamiltonian of the dimer also includes the SO coupling and Zeeman terms.

The energies of the CT states are defined by the Racah parameters of the Ti^{II} ion. In ref. 92 the values of the Racah parameters obtained for the free Ti^{II} ion have been used: $A = 141\,000\ cm^{-1}$, $B = 900\ cm^{-1}$, $C = 3300\ cm^{-1}$ (these values are close to those found in the cubic crystal field).[87] The parameter A plays the same role as the charge transfer energy U in Anderson's theory of the kinetic exchange. The value $\lambda = 155\ cm^{-1}$ was also used, which is the value of the SO coupling constant for the free Ti^{III} ion.[5]

Some remarks concerning the relative values of the transfer parameters t_a and t_e are now in order. First, the results of the extended Hückel calculations[124] demonstrated that $t_a^2 \gg t_e^2$ and t_e and t_a are of opposite signs. This result is consistent with the fact that the t_a transfer corresponds to the strong (due to the short intermetallic distance) through-space σ-interaction (Fig. 16), while the t_e transfer is responsible for a more weak interaction through the ligands. The conclusion about strong difference in the magnitudes of t_e and t_a has been confirmed by

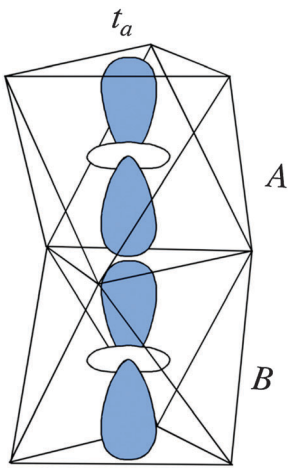

Fig. 16 Overlap scheme associated with the t_a transfer.

the *ab initio* calculation results in ref. 125. The ratio t_a/t_e was roughly estimated as $t_a/t_e \approx -6.5$. This corresponds to the ratio $t_e/t_a \approx -0.154$ which was used in the best fit procedure.

Finally, three parameters t_a, Δ_{trig} and κ were varied in course of fitting of the magnetic data, with Δ_{trig} being positive as described above. The parameter κ represents the orbital reduction factor that is involved in the SO-coupling term and orbital Zeeman term. The best fit was achieved for $t_a = -5208$ cm^{-1}, $\Delta_{trig} = -320$ cm^{-1} and $\kappa = 0.71$. The $\chi_{\parallel}$ *vs.* T and $\chi_{\perp}$ *vs.* T curves calculated with this set of parameters are shown in Fig. 15 along with the experimental data. One can see that the theoretical curve for $\chi_{\perp}$ is in a good agreement with the experimental data in the low-temperature region (below 170 K). The calculated $\chi_{\parallel}$ at low temperatures is also in satisfactory agreement with the experimental values. It is also remarkable that the theory well reproduces the slopes of $\chi_{\parallel}$ and $\chi_{\perp}$. Finally, it is seen that, in agreement with the experimental data, the calculated magnetic anisotropy remains constant below 100 K and decreases with the increase of T in the high-temperature region ($T > 150$ K).

Fig. 17 shows the energy scheme calculated (without spin-orbital splitting) for this system. The ground state is $^1A'_1$, and the first excited state $^3A''_2$ is separated by about 704 cm^{-1} from the ground one (a × a-group). The next four orbital doublets $^3E''$, $^1E''$, $^3E'$, and $^1E'$ (a × e-manifold) fill the gap ≈134 cm^{-1}. This group of levels is close to the level $^3A''_2$. Finally, the e × e-group of levels forms a narrow band that is about 1340 cm^{-1} higher than the ground $^1A'_1$ level. It should be mentioned that the trigonal crystal field splitting is relatively small and the exchange mixing of the two $^1A'_1$ states arising from a × a and e × e-multiplets is significant. This produces a strong stabilization of the diamagnetic ground level $^1A'_1$ and can be considered as a manifestation of the orbital effects. Inspection of this energy pattern allows us to qualitatively explain the observed magnetic behavior of the $[Ti_2Cl_9]^{3-}$ unit, at least at low temperatures. First, the ground state is the orbital and spin singlet $^1A'_1$ and in the absence of SO coupling there is no Zeeman mixing of this state with the excited ones in the parallel field (along C_3 axis). As a consequence, in parallel field both the first order Zeeman splitting and the TIP contribution vanish in the ground state and therefore $(\chi_{\parallel})_{T\to 0} = 0$. At the same time, $(\chi_{\perp})_{T\to 0}$ appears as a second order effect due to the mixing of the ground $^1A'_1$ term with the orbital doublets $^1E'$ and $^1E''$. The inclusion of the SO coupling leads to a small admixture of the magnetic states to the ground diamagnetic level resulting thus in the nonvanishing value of $(\chi_{\parallel})_{T\to 0}$.

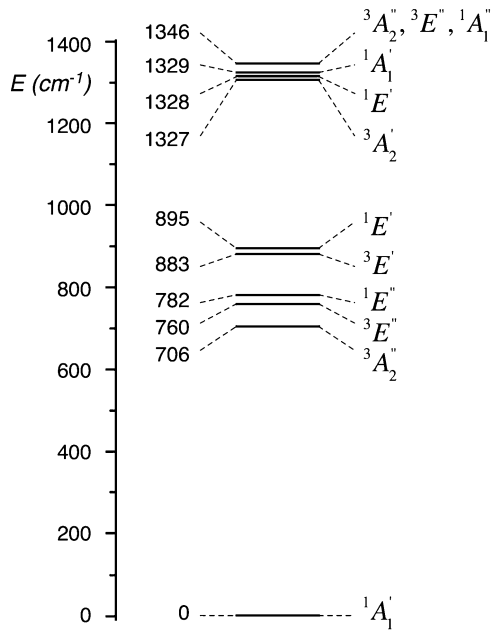

Fig. 17 Calculated energy pattern of the $[Ti_2Cl_9]^{3-}$ unit. Adapted from ref. 92.

The above analysis shows that the adequate description of the magnetic anisotropy of the $[Ti_2Cl_9]^{3-}$ unit requires a careful consideration of the orbital contribution. More detailed discussion of different rival models and approaches aimed to explain different aspects of the magnetic behavior of this system can be found in ref. 97 (see also references therein).

5.2. Orbitally-dependent exchange in rare-earth compounds $Cs_3Yb_2Cl_9$ and $Cs_3Yb_2Br_9$. Origin of its surprising isotropy

Most of the rare earth based compounds exhibit a very strong magnetic anisotropy that manifests itself both in local parameters (anisotropy of g-tensor) and in the anisotropy of the exchange.[127–131] A large amount of experimental data,[132–134] in conjunction with the clear physical concept about the role of the orbital angular momentum, led to a firm conviction that strong exchange anisotropy is an inherent and common property of the rare earth systems with unquenched orbital angular momenta. However, the rare-earth compounds $Cs_3Yb_2Cl_9$ and $Cs_3Yb_2Br_9$, which are formed by pairs of $YbCl_6$ octahedra sharing a face (D_{3h} symmetry), seem to be an exception from this general rule. In fact, the INS experiments of Güdel *et al.*[135] showed that the exchange interaction between Yb^{III} ions in these compounds seems to be isotropic and can be described by the Heisenberg type Hamiltonian acting within the lowest Kramers doublets of Yb^{III} ions. Conversely, a significant exchange anisotropy arising from the orbital degeneracy was found in numerous other systems including the isostructural compounds $Cs_3Ho_2Br_9$[134] and $YbCrBr_9$.[131] An attempt to understand the origin of this isotropy was made in ref. 136 where the effective-pseudo-spin-1/2 Hamiltonian describing the kinetic exchange between two octahedrally coordinated Yb^{III} ions in their ground Kramers doublet states have been deduced. The Hamiltonian derived in ref. 136 is expressed in terms of the operators defined with respect to the local frames, hence, it does not give a clear answer about the character of the exchange anisotropy (or isotropy). For this reason here we will mainly follow ref. 136 but the Hamiltonian will be expressed in terms of operators defined with respect to the molecular frame.

Since the local anisotropy (anisotropy of g-tensors of the constituent Yb^{III} ions) is weak in the systems under study, one can neglect the weak trigonal components of the crystal field and consider the idealized system built from two perfect octahedral Yb^{III} sites like in $[Ti_2Cl_9]^{3-}$ unit. The SO coupling in rare-earth ions is strong as compared to crystal field and

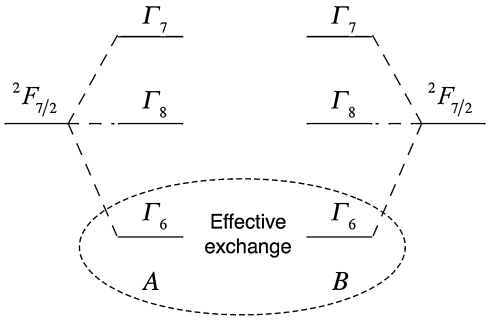

Fig. 18 Cubic crystal field splitting of the ground $^2F_{7/2}$ multiplet of the Yb^{III} ion and schematic image of the $\Gamma_6 \otimes \Gamma_6$ exchange problem.

stabilizes the $^2F_{7/2}$ term ($L = 3$, $S = 1/2$) as the ground state of Yb^{III}. The cubic crystal field splits the ground term $^2F_{7/2}$ of Yb^{III} ions into two Kramers doublets Γ_6 and Γ_7 and a quadruplet Γ_8 in such a way that the Kramers doublet Γ_6 proves to be the ground state (Fig. 18). Since the energy gap between the ground and excited states was shown to exceed considerably the exchange interaction,[135] one arrives at the $\Gamma_6 \otimes \Gamma_6$ exchange problem as schematically shown in Fig. 18.

Considering symmetry adapted combinations of the spherical harmonics $Y_{4m}(\theta,\varphi)$ one can build the wave-functions of the Kramers doublet from the $^2F_{7/2}$ manifold. Nevertheless, there is a more appropriate way to treat the problem of the magnetic exchange. Let us note that the 4f-atomic level is split in the cubic crystal field into two triplets, T_1 and T_2, and a singlet, A_2. Simple group–theoretical arguments show that Γ_6 arises only from T_1 orbital triplet when the last is coupled to the spin state with $S = 1/2$ (Γ_6). This means that only T_1-states contribute to the ground Kramers doublets.

The mechanism of the kinetic exchange between the lanthanide ions was proposed by Goodenough.[86] This mechanism deals with the electron transfer from the 4f-orbital of one rare-earth ion to the 5d-orbital of another one. Now along with the 4f-orbitals of T_1-type we have to use the 5d-orbitals that form the bases of T_2 and E irreducible representations in O-group.

Within a simplified model of the CT states the intraionic Coulomb repulsion between 4f and 5d electrons is approximated by one parameter U_{fd} that is assumed to include the spherical term $F^0(4f,5d)$ and the energy difference Δ_{fd} between 4f and 5d orbitals. The intra-center exchange is approximated by the only exchange integral $J_{fd} \approx G^1(4f,5d)$. This exchange discriminates the energies of spin triplets and spin singlets; the corresponding energy gap is equal to J_{fd}. In addition, the cubic crystal field splitting of the 5d levels, which is of the order of 10 $Dq \approx$ 2–3 eV, is taken into account.

The 4f $\leftrightarrow$ 5d electron transfer mixes the ground configuration $(4f^{13}5d^0)_A$–$(4f^{13}5d^0)_B$(g) with the two CT excited ones $(4f^{13}5d^1)_A$–$(4f^{12}5d^0)_B$ and $(4f^{12}5d^0)_A$–$(4f^{13}5d^1)_B$ (e).

It is reasonable to simplify the calculation taking into account only the strongest through-space direct σ–σ (4f $\leftrightarrow$ 5d) interaction involving the f_{a_1}-orbital of one center and the d_{a_2} orbital of the second center:

$$t_a = \langle f^A_{a_1}|\hat{H}_{tr}|d^B_{a_2}\rangle = \langle f^B_{a_1}|\hat{H}_{tr}|d^A_{a_2}\rangle, \qquad (40)$$

where f_{a_1} is the real trigonal t_1-type 4f-orbital having the form

$$f_{a_1} = \tfrac{5}{6\sqrt{2}}f_{X^3} - \tfrac{2}{3}f_{Z^3} + \tfrac{\sqrt{5}}{2\sqrt{6}}f_{X(Y^2-Z^2)}, \qquad (41)$$

and d_{a_2} is the real trigonal t_2-type 5d-orbital given by eqn (38). Within the adopted approximations the energies of the CT spin-triplets and spin-singlets will be $U_{fd} - J_{fd} - 4Dq = \tilde{U}_{fd} - J_{fd}$ and $U_{fd} + J_{fd} - 4Dq = \tilde{U}_{fd} + J_{fd}$, respectively, where $\tilde{U}_{fd} = U_{fd} - 4Dq$ is an effective Coulomb repulsion energy that takes into account the stabilization of the CT states due to the cubic crystal field splitting. Using the explicit expression for the matrix elements of the one-electron $4f_A \rightarrow 5d_B$ transfer operator connecting the ground and the CT states one finds the form $\hat{H}^{eff}_{ex} = -2J\hat{\tau}_A\hat{\tau}_B$ for the pseudo-spin-1/2 Hamiltonian in which $\hat{\tau}_A$ and $\hat{\tau}_B$ operators are defined in the molecular frame that is chosen to coincide with the local trigonal X_A,Y_A,Z_A frame (Fig. 14), and

$$J = \frac{t_a^2}{9(\tilde{U}_{fd} + J_{fd})} - \frac{t_a^2}{9(\tilde{U}_{fd} - J_{fd})}. \qquad (42)$$

One can see that the interaction between two Yb^{III} ions in their Kramers doublet states is antiferromagnetic ($J < 0$) and can be described by the isotropic HDVV Hamiltonian. These findings are in accordance with experimental data obtained in the INS study.[135]

5.3 A model for the spin-canted antiferromagnetic single-chain magnet $Co(H_2L)(H_2O)$ (L = 4-Me–C_6H_4–$CH_2N(CPO_3H_2)_2$)

In this section the importance of orbital contributions in the Co^{II} diphosphonate $Co(H_2L)(H_2O)$ chain compound will be demonstrated. This compound synthesized and magnetically characterized in ref. 137 is of interest for the following reasons: (i) it represents a SCM, the 1D system that behaves like a bulk magnet; (ii) this is a rare example of antiferromagnetic chain showing such a behavior; (iii) finally, in view of the topic of this review, this system is composed of the high-spin Co^{II} ions, which possess unquenched orbital angular momenta.

A slow relaxation of magnetization in SCMs appears due to the exchange interaction between fast relaxing units. A theoretical background for the description of SCM behavior is provided by Glauber's stochastic approach.[138] It was predicted a slow relaxation of the magnetization for a chain composed of ferromagnetically coupled Ising type spins 1/2. In Glauber's theory the thermal variation of the relaxation time τ is described by the Arrhenius low

$$\tau(T) = \tau_0 \exp\left(\frac{\Delta_b}{k_B T}\right), \qquad (43)$$

in which the barrier Δ_b for the reversal of magnetization represents the energy loss in a single spin flip-flop process, that is $\Delta_b = 2J$.

An Ising type spin chain can apparently behave as a SCM only if the constituent magnetic units are coupled in such a way that their magnetic moments are not compensated. In majority of known SCMs this condition is satisfied either due to a ferromagnetic interaction between the same spins or due to alternation of different antiferromagnetically coupled spins. Therefore a recently reported example of SCM composed of

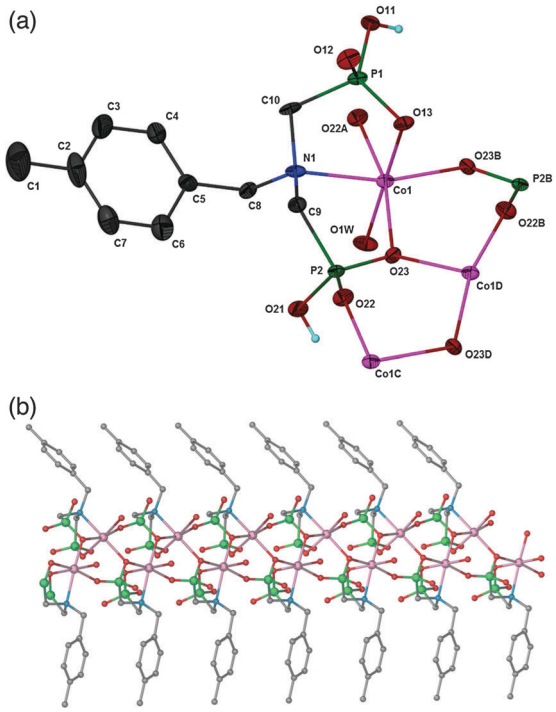

Fig. 19 (a) ORTEP representation of the $Co(H_2L)(H_2O)$ unit. The thermal ellipsoids are drawn at the 50% probability level. (b) An extension of the view in (a) looking down the *c*-axis to emphasize the zig-zag chain structure. The Co, P, N, O atoms are shaded in pink, green, blue and red respectively. Adapted from ref. 118.

antiferromagnetically coupled metal ions of the same kind[137] seems to be quite unusual. In this system the Co^{II} ions are linked through the bridging phosphonate oxygen atom to create a 1D chain of corner-shared octahedra which propagate in a zigzag fashion (Fig. 19). A quantum-mechanical approach to the description of the SCM behavior in this compound has been developed in ref. 118. It was demonstrated that the uncompensated magnetic moment at low temperatures is a result of the noncollinear spin structure (spin canting). In fact, the crystallographic positions of neighboring Co^{II} ions in the chain are inequivalent because the corresponding ligand octahedra are rotated with respect to each other;[137] precisely this situation results in a spin canting. At the same time the two cobalt centers in the chain have identical environments and are linked to five oxygen and one nitrogen atoms.

As pointed out before, the ground state of the high-spin Co^{II} ion in an ideal octahedral surrounding can be represented with a good accuracy by the only configuration $t_{2g}^5e_g^2$ that gives rise to the orbital triplet $^4T_{1g}(t_{2g}^5e_g^2)$ possessing fictitious orbital angular momentum $l = 1$. From the structure of the compound one observes that the nearest octahedral surroundings of the Co^{II} ions are strongly tetragonally distorted. Let us assign the indices A and B to two octahedrally coordinated Co^{II} ions which occupy inequivalent crystallographic positions in a 1D chain. Then, one has to introduce two local frames of reference (Fig. 20) relating to ions A and B in the chain. We assume that the tetragonal local Z_A and Z_B axes subtend an angle φ, the Y_A and Y_B axes are chosen to be parallel to each other and perpendicular to Z_AZ_B-plane, while the axes X_A and

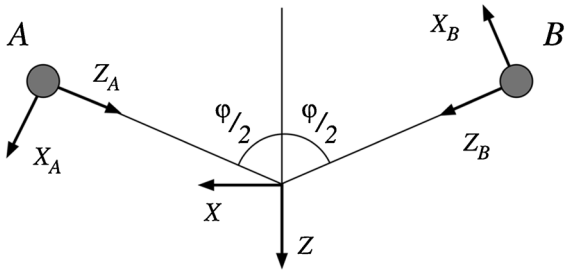

Fig. 20 Local and molecular frames. Adapted from ref. 92.

X_B lie in the Z_AZ_B-plane. The B center system axes can be obtained from the A center system axes by the φ degree turn around Y_A or Y_B axis. Along with the local frames, we will also use the molecular coordinates chosen in such a way that the molecular *Z* axis is directed along the bisector of the angle φ formed by the local Z_A and Z_B axes while the *Y* axis of the molecular system coincides with the local Y_A and Y_B axes as shown in Fig. 20.

The tetragonal component of the ligand field splits the ground $^4T_{1g}$ term of each Co^{II} ion into the orbital singlet $^4A_{2g}(m_l = 0)$ and the orbital doublet $^4E_g(m_l = \pm 1)$. Depending on the sign of the tetragonal crystal field, either the orbital singlet or the orbital doublet can become the ground state. However, as was demonstrated in ref. 118 only the ground orbital doublet $^4E_g(m_l = \pm 1)$ is compatible with the SCM behavior of the system under consideration.

A reasonable assumption that directly follows from the overall symmetry of the corner-shared bioctahedral unit is that the only transfer pathway significantly contributing to the kinetic exchange is that associated with $3Z_A^2–r_A^2$ and $3Z_B^2–r_B^2$ -orbitals, which are directed towards the bridging oxygen ligand and thus can efficiently overlap. The orbital scheme illustrating the kinetic exchange in the Co^{II} pair is shown in Fig. 21. It is seen that, in the case under consideration, we are

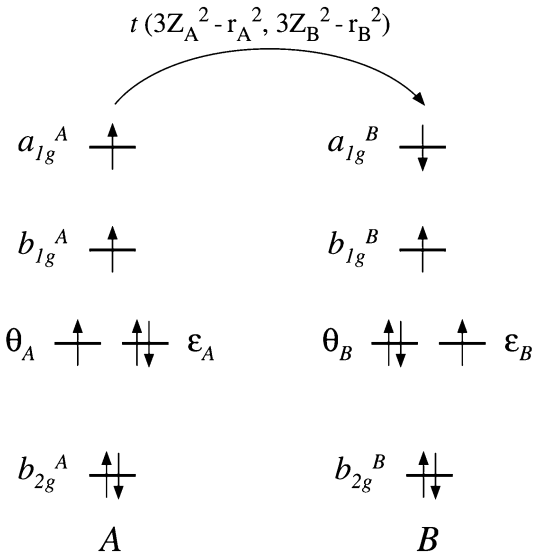

Fig. 21 Orbital scheme showing the kinetic exchange mechanism for two Co^{II} ions occupying tetragonally distorted octahedral positions. Only one of four microstates belonging to the ground manifold is shown ($b_{2g} \propto XY$, $\theta_A \propto YZ$, $\varepsilon_A \propto XZ$, $b_{1g} \propto X^2–Y^2$, $a_{1g} \propto 3Z^2–r^2$).

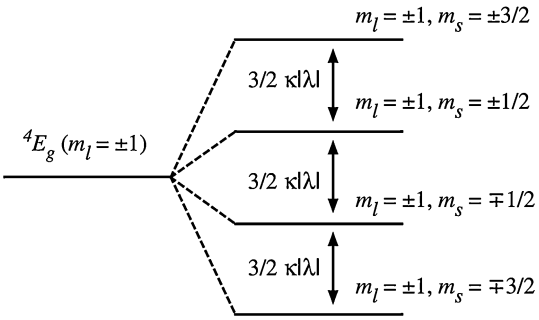

Fig. 22 Splitting of the ground tetragonal ^{4}E term by the SO coupling.

dealing with the electron transfer between the orbitally non-degenerate orbitals a_{1g}^{A} and a_{1g}^{B}, and hence, according to the rule established in Section 4.2 the kinetic exchange can be described by the isotropic pseudo-Heisenberg Hamiltonian $\hat{H}_{ex} = -2J\hat{s}_A\hat{s}_B$. Assuming that the splitting caused by the tetragonal ligand field considerably exceeds the SO splitting (axial limit) and neglecting the SO mixing of the ^4E_g and $^4A_{2g}$ terms one arrives at the scheme of the low-lying energy levels of the Co^{II} ion as shown in Fig. 22. Within the ground ^4E_g term the SO interaction takes on the axial form

$$\hat{H}_{SO}(^4E_g) = -(3/2)\,\kappa\lambda\hat{l}_Z\hat{s}_Z. \qquad (44)$$

The SO coupling leads to the splitting of the ^4E_g term into four equidistant Kramers doublets, with the doublet possessing $m_l = \pm1$, $m_s = \mp3/2$ being the ground one (Fig. 22). The SO splitting considerably exceeds the exchange interaction in the $Co(H_2L)(H_2O)$ unit and hence the pseudo-spin-1/2 Hamiltonian formalism for the ground Kramers doublet is a well justified approximation. To define this Hamiltonian let us first present the isotropic pseudo-Heisenberg Hamiltonian in the form

$$\hat{H}_{ex} = -2J[\hat{s}_X(A)\hat{s}_X(B) + \hat{s}_Y(A)\hat{s}_Y(B) + \hat{s}_Z(A)\hat{s}_Z(B)], \qquad (45)$$

where the single ion spin operators $\hat{s}_\gamma(A)$ and $\hat{s}_\gamma(B)$ ($\gamma = X,Y,Z$) refer to the molecular frame. Then one should pass from the operators $\hat{s}_\gamma(A)$, $\hat{s}_\gamma(B)$ to the operators $\hat{s}_{\gamma A}$, $\hat{s}_{\gamma B}$ defined in the local coordinates. Performing this transformation with the aid of the rotation matrices one obtains:

$$\hat{H}_{ex} = -2J[\hat{s}_{Y_A}\hat{s}_{Y_B} + \cos(\varphi)(\hat{s}_{X_A}\hat{s}_{X_B} + \hat{s}_{Z_A}\hat{s}_{Z_B}) - \sin(\varphi)(\hat{s}_{X_A}\hat{s}_{Z_B} - \hat{s}_{Z_A}\hat{s}_{X_B})]. \qquad (46)$$

All matrix elements of the operators $\hat{s}_{X_A}$, $\hat{s}_{Y_A}$, $\hat{s}_{X_B}$ and $\hat{s}_{Y_B}$ are vanishing within the ground Kramers doublet and hence the initial pseudo-Heisenberg Hamiltonian is reduced to the Ising form

$$\hat{H}_{ex}^{eff} = -2J_{eff}\,\hat{\tau}_{Z_A}\hat{\tau}_{Z_B}, \qquad (47)$$

where $\hat{\tau}_{Z_A}$, $\hat{\tau}_{Z_B}$ are the pseudo-spin-1/2 operators, and the effective exchange parameter is

$$J_{eff} = 9J\cos(\varphi)\left[1 - \frac{J\cos(\varphi)}{3\kappa|\lambda|}\right]. \qquad (48)$$

The pseudo-spin-1/2 basis is chosen in such a way that the components of the ground Kramers doublet level with $m_l = -1$, $m_s = 3/2$ ($m_l = 1$, $m_s = -3/2$) corresponds to the projection $\sigma = 1/2$ ($\sigma = -1/2$) of the pseudo-spin-1/2. As a result, the effective single ion pseudo-spin-1/2 Hamiltonian is found to be:[117]

$$\hat{H}_i^{eff} = g_{||}\beta\hat{\tau}_{Z_i}H_{Z_i} - \Lambda_\perp(H_{X_i}^2 + H_{Y_i}^2), \quad i = A, B, \qquad (49)$$

where $g_{||} = 3(\kappa + g_e)$, $g_\perp = 0$ are the principal values of the g-tensor for the Co^{II} ion, and $\Lambda_{||} = 0$, $\Lambda_\perp = g_e^2\beta^2/2\kappa|\lambda|$ are the principal values of the tensor of the TIP. The TIP contribution appears as a result of the Zeeman mixing of the ground Kramers doublet with the three lowest excited states.

Using these results one can write down the following total Hamiltonian for a chain including exchange interaction between nearest neighboring Co^{II} ions and Zeeman terms (excluding TIP):

$$\hat{H}^{eff} = -2J_{eff}\sum_i\{[\hat{\tau}_{Z_A}(i)\hat{\tau}_{Z_B}(i) + \hat{\tau}_{Z_B}(i)\tau_{Z_A}(i+1)]\} + g_{||}\beta[\hat{\tau}_{Z_A}(i)H_{Z_A} + \hat{\tau}_{Z_B}(i)H_{Z_B}]\}, \qquad (50)$$

where index i numbers the AB pairs. In eqn (42) both the spin operators and the components of the magnetic field are defined in the local frames.

It is to be noted that the Ising form of the effective Hamiltonian is only valid if the pseudo-spin-1/2 operators are defined in the local frames. In the molecular frame the exchange Hamiltonian does not retain the Ising form. Nevertheless formal similarity between the Hamiltonian, eqn (50), and true Ising Hamiltonian provides a straightforward way to find the interrelation between the height of the magnetic barrier and the exchange parameter. Let us consider, for example, a single spin flip-flop process in the absence of the magnetic field, for which one spin (let us say, the spin of the center B in the first AB pair) is overturned

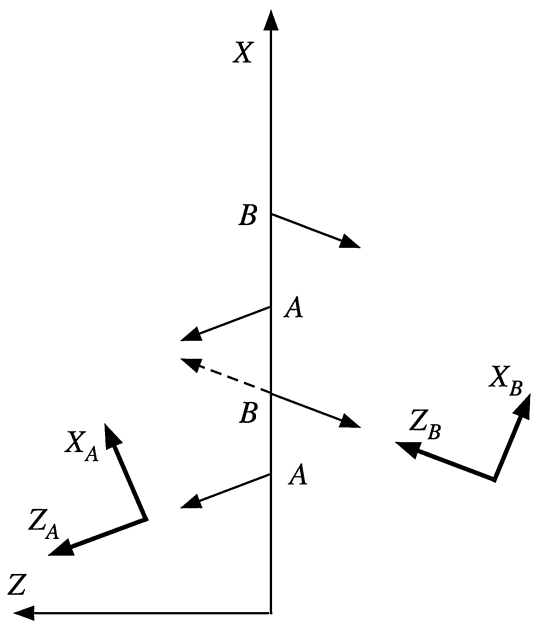

Fig. 23 Noncollinear spin structure of the chain and illustration for a spin flip-flop process. Adapted from ref. 92.

(Fig. 23). It follows from eqn (50) that the energy loss in such a process can be calculated as

$$\begin{aligned}\Delta_b &= E[\sigma_A(1) = \pm\tfrac{1}{2}, \sigma_B(1) = \mp\tfrac{1}{2}, \sigma_A(2) = \pm\tfrac{1}{2}, \sigma_B(2) \\ &= \mp\tfrac{1}{2}, \sigma_A(3) = \pm\tfrac{1}{2}, \sigma_B(3) = \mp\tfrac{1}{2}, \ldots] - E[\sigma_A(1) \\ &= \pm\tfrac{1}{2}, \sigma_B(1) = \pm\tfrac{1}{2}, \sigma_A(2) = \pm\tfrac{1}{2}, \sigma_B(2) = \mp\tfrac{1}{2}, \sigma_A(3) \\ &= \pm\tfrac{1}{2}, \sigma_B(3) = \mp\tfrac{1}{2}, \ldots] = 2|J_{eff}|, \end{aligned} \quad (51)$$

where all spin-projections are defined in the local frames. One thus obtains the same relation as that derived from the true Ising Hamiltonian. An analytical solution for the magnetic susceptibility of a chain described by this effective Hamiltonian, eqn (50), can be derived. The details of this calculation can be found in ref. 118.

The temperature dependence of the relaxation time for the $Co(H_2L)(H_2O)$ compound can be obtained from the frequency dependence of the in-phase (χ') and out-of-phase (χ'') ac susceptibility. The experimental and calculated $\ln(1/\tau)$ *vs.* $1/T$ dependences are shown in Fig. 24. The best fit parameters were found to be $\Delta_b(\chi') = 18.6\ cm^{-1}$, $\tau_0(\chi') = 3.4 \times 10^{-9}$ s for the in-phase signal of frequency-scan and $\Delta_b(\chi'') = 20.2\ cm^{-1}$, $\tau_0(\chi'') = 8.4 \times 10^{-10}$ s for the out-of-phase signal, respectively. Then, considering a simple average $\Delta_b = [\Delta_b(\chi') + \Delta_b(\chi'')]/2 = 19.4\ cm^{-1}$ as a reasonable value of the barrier height one finds from eqn (51) that $J_{eff} = -9.7\ cm^{-1}$.

Magnetic susceptibility measurements performed on a polycrystalline sample of the compound at the field $H = 0.1$ T over the temperature range 2–50 K (Fig. 25) gave the χT *vs.* T curve that is quite similar to that observed in the ferrimagnetic spin chains. As the temperature is lowered, the χT value decreases and reaches a minimum of 0.6 emu K mol^{-1} at 7 K. Below 7 K, the χT increases abruptly to reach a maximum at ~2.5 K ($\chi T_{max} = 2.5$ emu mol^{-1} K) and finally decreases again at lower temperatures. The observed increase of χT below 7 K can be obviously explained by the fact that antiferromagnetic exchange does not lead to perfect cancellation of spins due to spin canting. In the calculation of χT it is reasonable to use the values $\lambda = -180\ cm^{-1}$, $\kappa = 0.8$ that are typical for the high-spin Co^{II} ion, and the effective exchange parameter value $J_{eff} = -9.7\ cm^{-1}$ obtained from the Arrhenius plot. The angle φ between the easy anisotropy axes of A and B ions are allowed to be changed in course of the fitting to the experimental χT *vs.* T curve. The best fit is achieved for the angle $\varphi = 15°$. Fig. 25 shows a close agreement between the observed and calculated χT *vs.* T curves, thus indicating that the theory adequately describes both dynamic and static magnetic properties of the compound.

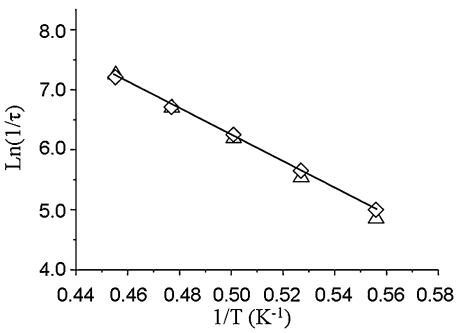

Fig. 24 Temperature dependence of the relaxation time. The triangles and diamonds represent the relaxation time obtained from frequency dependence of x' and x'', respectively. The solid line corresponds to the best fit of the data to the Arrhenius low. Adapted from Ref. 137.

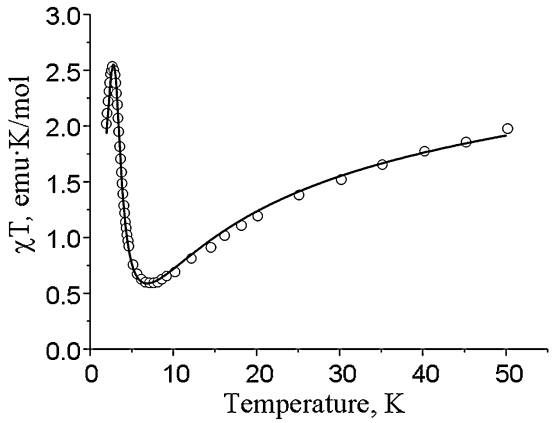

Fig. 25 Temperature dependences of χT for $Co(H_2L)(H_2O)$ compound: triangles—experimental data reported in ref. 137, solid line—theoretical curve calculated in ref. 118 with $\lambda = -180\ cm^{-1}$, $\kappa = 0.8$, $J_{eff} = -9.7\ cm^{-1}$ and $\varphi = 15°$. Adapted from ref. 118.

5.4 Pseudo-spin-1/2 Hamiltonian approach for the trigonal bipyramidal cyano-bridged $Ni^{II}_3Os^{III}_2$ complex

Recently the synthesis and magnetic properties of a new complex $\{[Ni^{II}(tmphen)_2]_3[Os^{III}(CN)_6]_2\}\cdot 6CH_3CN$ ($Os^{III}_2Ni^{II}_3$ cluster) with a pentanuclear trigonal bipyramidal structure[139] (Fig. 26) has been reported. The ground state of the Ni^{II} ion in the octahedral surrounding of the N-bound cyanide ligands is the orbital singlet $^3A_{2g}(t_{2g}^6e_g^2)$. A strong cubic crystal field induced by six C-bound cyanides gives rise to the triply degenerate ground term $^2T_{2g}(t_{2g}^5)$ for the Os^{III} ion that is the state with $l = 1$. Each Os^{III} ion in this cluster is magnetically coupled with three Mn^{II} ions *via* the superexchange mediated by the cyanide bridges. The structure of this system is quite similar to that previously reported for trigonal bipyramidal cyano-bridged cluster $[Mn^{III}(CN)_6]_2[Mn^{II}(tmphen)_2]_3$ (tmphen = 4, 5, 7, 8-tetramethyl-1,10-phenanthroline), which contain two orbitally degenerate low-spin Mn^{III} ions coupled with three orbitally non-degenerate Mn^{II} through magnetic exchange[140] (this system will be discussed later on). However, in spite of their similarity, these two systems exhibit quite different magnetic behavior. In fact, the $Mn^{III}_2Mn^{II}_3$ cluster was found to exhibit slow relaxation of the magnetization, a property that is typical for SMMs. As distinguished from the $Mn^{III}_2Mn^{II}_3$ cluster the $Os^{III}_2Ni^{II}_3$ system does not show SMM behavior. This remarkable observation can be understood within a model developed for $Ni^{II}_3Os^{III}_2$, which takes into account orbital degeneracy of the low-spin Os^{III} ions and the complex molecular structure of this compound.[120]

The crystal structure analysis reveals that the $Ni^{II}_3Os^{III}_2$ cluster consists of two axial $[Os(CN)_6]^{3-}$ units connected *via* bridging cyanide ligands to three equatorial $[Ni(tmphen)_2]^{2+}$ moieties to yield a trigonal bipyramidal geometry (Fig. 26). The Os–CN bond lengths and CN–Os–CN bond angles exhibit nearly perfect octahedral symmetry of the $[Os(CN)_6]^{3-}$ fragments. These fragments are not crystallographically

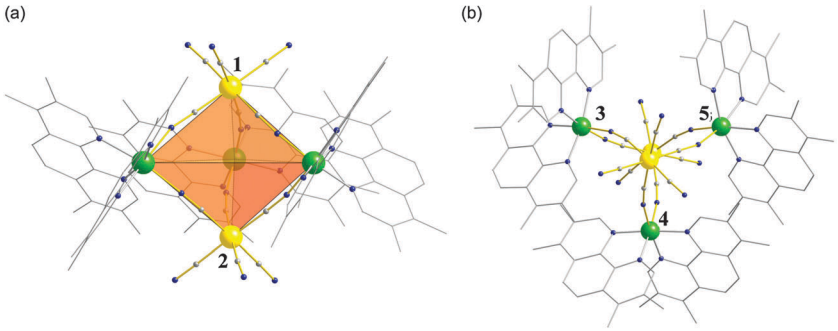

Fig. 26 Molecular structure of the Ni_3Os_2 complex with the numbering of metal ions: (a) a side view emphasizing the NiN_6 and OsC_6 coordination environments; the trigonal bipyramidal cluster core is highlighted with a hypothetical polyhedron; (b) a view along the axis of the trigonal bipyramid emphasizing the approximately trigonal symmetry around each Os site. To allow for a better view of the cluster core, the tmphen ligands are shown in the stick mode and the H atoms are omitted. Color scheme: Ni = green; Os = yellow; N = blue; C = gray. Adapted from ref. 120.

equivalent, but an inspection of their coordination geometry shows that Os^{III} centers are very similar and can be described with one set of magnetic parameters to avoid over-parametrization.

The model proposed in ref. 120 explicitly takes into account the strong SO coupling acting within the $^2T_{2g}(t_{2g}^5)$ term of the Os^{III} ion. The SO coupling splits this term into the Kramers doublet Γ_7 and quadruplet Γ_8, with the doublet $\Gamma_7(\pm 1/2)$ being the ground state. Since the energy gap between the Γ_7 and Γ_8 levels for the osmium ions exceeds 5000 cm^{-1},[141] the ground Γ_7 doublet of the Os^{III} ion is well separated from the remaining part of the energy pattern. In this case, the exchange Hamiltonian describing the low-lying levels includes pseudo-spin-1/2 operators related to two Os^{III} ions and true spin-1 operators related to three Ni^{II} ions for which the orbital contribution is very small. This Hamiltonian is expected to describe the magnetic data for the $Ni^{II}{}_3Os^{III}{}_2$ cluster up to room temperature.

The effective g-factor for the Kramers doublet $\Gamma_7(\pm 1/2)$ of the Os^{III} ion in an ideal octahedral ligand field is $g_{eff}(Os) = (ge + 4\kappa)/3$. The value $\kappa = 0.66$ was obtained in ref. 141 by fitting the magnetic data and electronic absorption spectra for the free $[Os(CN)_6]^{3-}$ anion. This value of κ gives $g_{eff}(Os) = 1.55$ which can be used in the calculations of the magnetic susceptibility data for the $Ni^{II}{}_3Os^{III}{}_2$ cluster. In order to avoid overparametrization, it is reasonable to take into account only the magnetic anisotropy arising from the orbitally-dependent exchange between Os^{III} and Ni^{II} ions and to neglect the less important single-ion anisotropic contributions like zero-field splitting of the spin levels of Ni^{II} ions and the anisotropy of the g-factor for Ni^{II} ions (typical value of $g(Ni) = 2.2$).

There are two possible pathways for the electron transfer processes between Os^{III} and Ni^{II} ions that contribute to the overall kinetic exchange: (1) the $t_{2g}^B \rightarrow t_{2g}^A$-transfer from the double occupied ξ or η-orbital of the Ni^{II} ion to the single occupied ξ or η-orbital of the Os^{III} ion through the bonding π and antibonding π^* orbitals of the cyanide ion (π-transfer associated with the overlap scheme shown in Fig. 27); (2) the $e_g^B \rightarrow e_g^A$-transfer from the single occupied u orbital of the Ni^{II} ion to the empty u orbital of the Os^{III} ion through the σ-orbitals of the cyanide bridge (σ-transfer). These two processes are shown in Fig. 28.

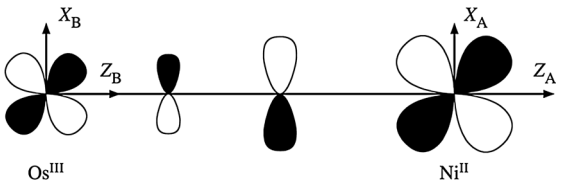

Fig. 27 Scheme of overlap between t_2 orbitals of Os^{III} and Ni^{II} through the π orbitals of the cyanide bridge.

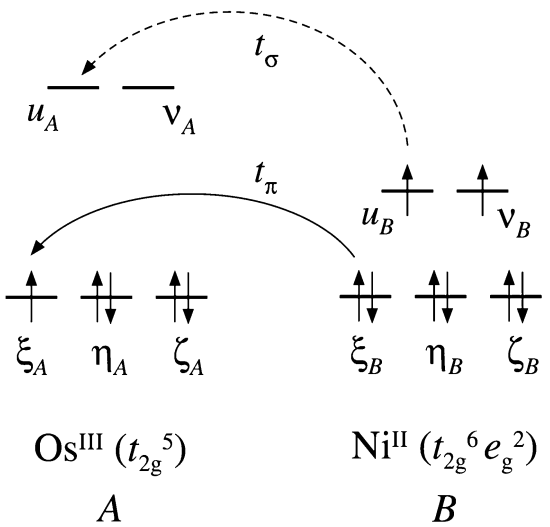

Fig. 28 Schemes of π and σ-contributions to the kinetic exchange in the $Os^{III}Ni^{II}$ pair.

Let us first analyze the π-transfer contribution to the kinetic exchange. Note that the $\Gamma_7(t_{2g}^5) \otimes {}^3A_{2g}(t_{2g}^6 e_g^2)$ exchange problem with the participation of π-transfer is quite similar to the model system $\Gamma_7(t_{2g}^5) \otimes {}^2B_{2g}(e_g^4 b_{2g}^1)$ examined in Section 4.3. In fact, in both cases we are dealing with the Kramers doublet state for the ion A, while the center B is orbitally nondegenerate. For this reason the Ising form of the effective exchange pseudo-spin-1/2 Hamiltonian that is found for the $\Gamma_7(t_{2g}^5) \otimes {}^2B_{2g}(e_g^4 b_{2g}^1)$-problem is also valid when the exchange between Os^{III} and Ni^{II} ions with the participation of the π-transfer is considered. One thus can write the Ising

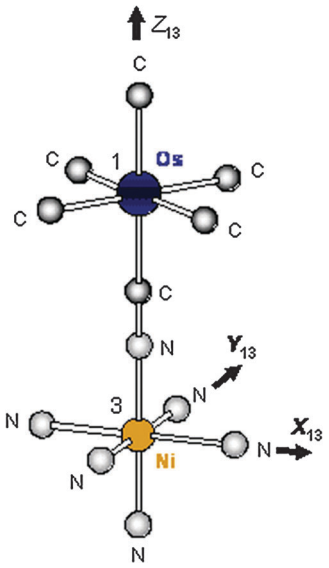

Fig. 29 Local frame for $(NC)_5Os(\mu\text{-}CN)NiN_5$ bioctahedral fragment.

Hamiltonian describing the π-contribution to the kinetic exchange for each $Os^{III}Ni^{II}$ pair in the cluster. For example, for Os(1)–Ni(3) pair one obtains

$$\hat{H}_{\pi}^{\text{eff}}(1,3) = -2J_{\parallel}(\pi)\hat{\tau}_{Z_{13}}(1)\hat{s}_{Z_{13}}(3), \qquad (52)$$

where $\hat{\tau}_{Z_{13}}(1)$ is the Z-component of the pseudo-spin-1/2 operator related to the ground Kramers doublet of the Os^{III} ion, and $\hat{s}_{Z_{13}}(3)$ represents the Z-component of the true spin operator for the Ni^{II} ion ($s_3 = 1$). These operators are defined in the local frame of the Os(1)–Ni(3) pair as shown in Fig. 29. The parameter $J_{\parallel}(\pi)$ is positive because the electron is transferred from the double-occupied orbitals of the Ni^{II} ion to the single-occupied orbital of the Os^{III} ion, and such a transfer gives rise to a ferromagnetic splitting according to the Goodenough–Kanamori rules.

Another kinetic exchange process associated with the σ-transfer gives rise to the isotropic pseudo-Heisenberg Hamiltonian for the $^5T_{2g}(t_{2g}^5) \otimes {}^3A_{2g}(t_{2g}^6e_g^2)$ exchange problem. In fact, this transfer process links two orbitally non-degenerate e_g-subshells of the constituent ions, namely the empty $^1A_{1g}(e_g^0)$-subshell of the Os^{III} ion and half-occupied $^3A_{2g}(e_g^2)$-subshell of the Ni^{II} ion. According to the general rule formulated in Section 4.2 such a transfer should lead to an isotropic pseudo-Heisenberg interaction between the true spins $s_{Os} = 1/2$ and $s_{Ni} = 1$ and hence to the isotropic Heisenberg effective pseudo-spin-1/2 Hamiltonian acting within the $\Gamma_7(t_{2g}^5) \otimes {}^3A_{2g}(t_{2g}^6e_g^2)$ manifold. Therefore, for a selected pair one can write down the following Hamiltonian:

$$\hat{H}_{\sigma}^{\text{eff}}(1,3) = -2J(\sigma)\hat{\tau}(1)\hat{s}(3). \qquad (53)$$

Again, and in accordance with the Goodenough–Kanamori rules, $J(\sigma) > 0$ since this contribution is associated with the electron transfer from the single-occupied u_B orbital to the empty u_A orbital. The total effective exchange Hamiltonian for the Os(1)–Ni(3) pair contains π and σ-contributions:

$$\hat{H}_{\text{ex}}^{\text{eff}}(1,3) = -2J_{\parallel}\hat{\tau}_{Z_{13}}(1)\hat{s}_{Z_{13}}(3) - 2J_{\perp}[\hat{\tau}_{X_{13}}(1)\hat{s}_{X_{13}}(3) + \hat{\tau}_{Y_{13}}(1)\hat{s}_{Y_{13}}(3)], \qquad (54)$$

where the exchange parameters are given by:

$$J_{\parallel} = J_{\parallel}(\pi) + J(\sigma), \quad J_{\perp} = J(\sigma). \qquad (55)$$

The density functional theory calculations of the exchange parameters in cyano-bridged species[142] demonstrated that the interaction through the cyanide σ-orbitals is significantly smaller as compared to the interaction through the π and π* orbitals. For this reason one can expect that $J_{\parallel}(\pi) \gg J(\sigma)$ and thus $J_{\parallel} \gg J_{\perp}$. In addition as follows from eqn (53), both $J_{\parallel}$ and $J_{\perp}$ are positive. The Hamiltonians for the Os(1)–Ni(4), Os(1)–Ni(5), Os(2)–Ni(3), Os(2)–Ni(4) and Os(2)–Ni(5) pairs can be written in a similar way.

On the basis of single crystal X-ray data for the $Ni^{II}{}_3Os^{III}{}_2$ complex, one can simplify the subsequent analysis assuming an idealized D_{3h} symmetry of the cluster. This assumption treats the complex as a perfect trigonal bipyramid in which the Ni triad forms an equilateral triangle and the trigonal axis passes through the apical Os(1) and Os(2) ions. To simplify calculations, one can assume that each Os–CN–Ni fragment has a linear arrangement.

In order to construct the total Hamiltonian of the $Ni^{II}{}_3Os^{III}{}_2$ cluster one has to pass from the operators defined in the local frames to the operators defined in the molecular frame, and to perform a summation over all Os–Ni pairs (see ref. 120 for the details). The parameters of this Hamiltonian are the functions of the exchange integrals $J_{\parallel}$ and $J_{\perp}$ and the angle θ between the Z_{13} and Z axes. Within the adopted idealized geometry, the angle θ is equal to 54.7°.

The experimental χT *vs.* T data for the powder sample reported in ref. 139 are shown in Fig. 30. It was observed that, as expected, the $Ni^{II}{}_3Os^{III}{}_2$ cluster exhibits ferromagnetic coupling between the Ni^{II} and Os^{III} centers. A plot of χT *vs.* T shows a slight increase as the temperature decreases reaching a maximum of 5.29 emu K mol^{-1} at 21.6 K; below this temperature χT decreases abruptly upon cooling. The two exchange parameters $J_{\parallel}$ and $J_{\perp}$ and also the TIP contribution, χ_{TIP}, to the magnetic susceptibility are allowed to vary during the fitting procedure, but with the restricting condition that $J_{\parallel} \gg J_{\perp} > 0$. The best fit parameters are found to be $J_{\parallel} = 23.8\ cm^{-1}$, $J_{\perp} = 1.2\ cm^{-1}$ and $\chi_{TIP} = 1.4 \times 10^{-3}\ cm^{-1}$.

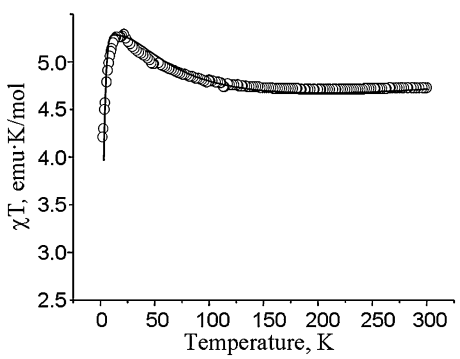

Fig. 30 Comparison of the experimental (red circles) and theoretical (blue line) χT *vs.* T curves for the powder sample of $Ni^{II}{}_3Os^{III}{}_2$. The theoretical curve was calculated with the set of the best fit parameters. The g-factors were fixed to $g_{\text{eff}}(Os) = 1.55$ and $g(Ni) = 2.2$. Adapted from ref. 120.

One can see that the use of this set of the parameters allows us to reproduce well the magnetic behavior of this cluster (Fig. 30).

The temperature dependence of $\chi_{\parallel}T$ and $\chi_{\perp}T$ calculated with the best-fit parameters indicates that $\chi_{\perp} > \chi_{\parallel}$, which means that the trigonal Z axis of the bipyramid is the hard axis of magnetization (or easy Ni^{II}_3 plane of magnetization). It is worth noting that the magnetic anisotropy with $\chi_{\perp} > \chi_{\parallel}$ precludes the existence of a barrier for the magnetization reversal in the $Ni^{II}_3Os^{III}_2$ cluster. This explains the fact that, in contrast to the trigonal bipyramidal $Mn^{III}_2Mn^{II}_3$ cluster which represents a SMM, the $Ni^{II}_3Os^{III}_2$ cluster is barrierless and therefore does not exhibit SMM behavior.

5.5 Polyoxometalates encapsulating Co^{II} clusters: inelastic neutron scattering study based on pseudo-spin-1/2 Hamiltonian

As has been illustrated in previous sections the presence of orbital degeneracy often leads to overparametrized exchange models. Hence, in these cases, the indirect information extracted from thermodynamic techniques (magnetic susceptibility and specific heat) is insufficient to obtain reliable values for the electronic and magnetic parameters. It is then mandatory to have more direct information about the energy splitting caused by the exchange and about the nature of the wave functions. In this section we show that the spectroscopic technique of the Inelastic Neutron Scattering (INS) can provide this kind of information.

In a series of recent works[111–115] the INS technique was applied to the study of the magnetic exchange in dinuclear, trinuclear and tetranuclear Co^{II} units. The first example of this kind represents the Keggin derivative $K_8[Co_2(D_2O)(W_{11}O_{39})]\cdot nD_2O$.[111] Encapsulation of two Co^{II} ions in the Keggin structure leads to the dimer shown in black in Fig. 31. The two Co^{II} ions in this complex are inequivalent. The divalent high-spin octahedral cobalt ion has a $^4T_{1g}$ ground state split into six Kramers doublets by the SO coupling and the low-symmetry crystal field, with the ground Kramers doublet (effective spin $\tau_1 = 1/2$) being the only level significantly populated below 30 K. This ground Kramers doublet can be described by the effective spin. The divalent cobalt ion in the tetrahedral environment has a ground orbital singlet $^4A_2$ with spin $s_2 = 3/2$.

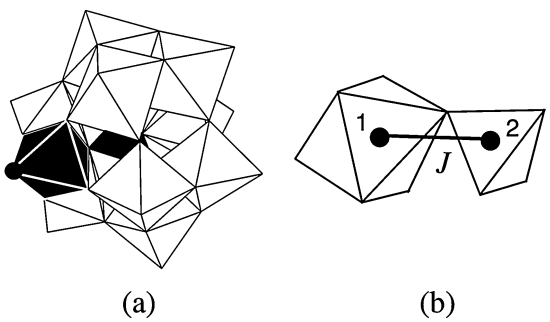

Fig. 31 (a) The structure of the $K_8[Co_2(D_2O)(W_{11}O_{39})]$ complex. The black polyhedra contain an oxo coordinated Co^{II} ions, and the white octahedra contain an oxo coordinated W atoms. (b) Octahedral-tetrahedral Co^{II} pair coupled through the magnetic exchange.

The effective Hamiltonian describing the exchange interaction between two Co^{II} ions can be written as

$$\hat{H}_{ex} = -2J[\hat{\tau}^1_Z\hat{s}^2_Z + \eta(\hat{\tau}^1_X\hat{s}^2_X + \hat{\tau}^1_Y\hat{s}^2_Y)]. \quad (56)$$

It should be emphasized that this Hamiltonian describes the interaction between the pseudo-spin-1/2 (Kramers doublet) and true spin 3/2. Providing $\eta \neq 1$, only the total angular momentum projection M_J (but not the total angular momentum J) is a good quantum number and the eigenvectors of the Hamiltonian, eqn (56), are given by the following linear combinations:

$$\psi_n(M_J) = \sum_J a_n(J, M_J)|\tau_1, s_2, J, M_J\rangle, \quad (57)$$

where index n is introduced to distinguish different states with the same M_J value.

The details of the calculation of neutron cross section are given in ref. 143 in which the relative INS intensities for all allowed $|\psi_n(M_J)\rangle \rightarrow |\psi_{n'}(M'_J)\rangle$ transitions have been found. These intensities as well as their Q-dependence provide information about the nature of the wave functions. On the other hand, INS spectra measured with cold neutrons (Fig. 32) and that measured with thermal neutrons of $\lambda = 2.44$ Å (see Fig. 4 in ref. 111) provide the energy level diagram shown in the left side part of Fig. 33. The best fit parameters are: $J = -2.24$ meV, $\eta = 0.33$. The value of the anisotropy parameter $\eta = 0.33$ indicates that the situation is intermediate between the Heisenberg ($\eta = 1$) and the Ising ($\eta = 0$) limits, and it is closer to the Ising one. The right-hand side of Fig. 33 shows the energy levels and corresponding wave-functions calculated with this set of parameters. The obtained best fit parameters were further used to calculate the temperature dependence of the magnetic susceptibility. In this calculation the g value for the tetrahedral Co^{II} ion was assumed to be equal to 2, for the octahedral site the ratio $\eta = g_{\perp}/g_{\parallel}$ was fixed, and $g_{\perp}$ was the only adjustable parameter. The best fit to the experimental χT *vs.* T curve was achieved for $g_{\perp} = 2.3$ that corresponds to $g_{\parallel} = 7.0$. The χT *vs.* T curve calculated with this set of parameters is in excellent agreement with the

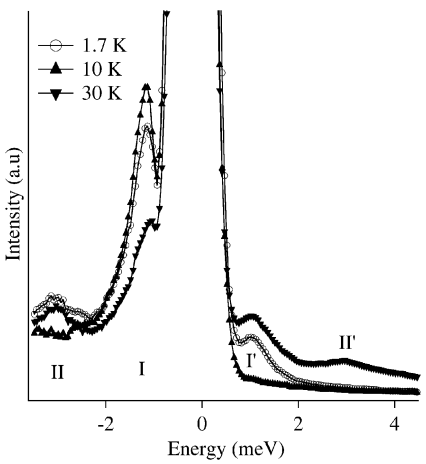

Fig. 32 Inelastic neutron scattering INS spectra with cold neutrons. The measurements were performed at temperatures of 1.7, 10 and 30 K with incident neutron wavelength $\lambda = 4.1$ Å.

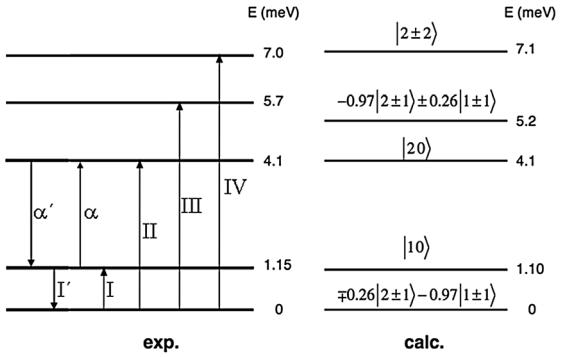

Fig. 33 Experimentally determined energy pattern $K_8[Co_2(D_2O)\text{-}(W_{11}O_{39})]$ material (left) and that calculated with the best fit parameters $J = -2.24$ meV, $\eta = 0.33$ (right). The observed cold (I, II, III, IV) and hot (α, α′, I′) transitions and the calculated wave-functions are shown.

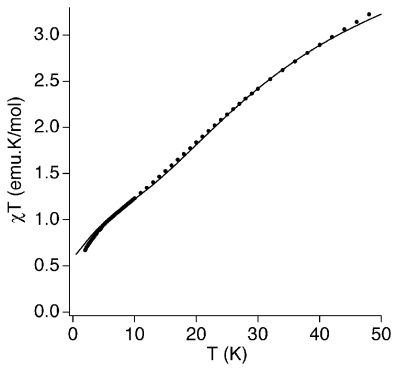

Fig. 34 Measured magnetic susceptibility of a polycrystalline sample measured between 2 and 50 K (full circles) and χT *vs.* T curve calculated with the set of parameters: $J = -2.24$ meV, $\eta = 0.33$, $g_\perp = 2.3$ $g_\parallel = 7.0$/(solid line).

experimental data (Fig. 34). The obtained $g_\parallel$ and $g_\perp$ are reasonable g-values for a Co^{II} site with a slightly distorted octahedral coordination.

Later on the exchange interaction in the tetranuclear cobalt containing cluster $[Co_4(H_2O)_2(PW_9O_{34})_2]^{10-}$ was studied with the aid of INS technique combined with the analysis of thermodynamic properties, including specific heat and magnetic susceptibility.[112] The structure of this compound is shown in Fig. 35. It represents a tetrameric rhomblike centrosymmetrical cluster Co_4O_{16} of D_{2h} symmetry formed by four coplanar edge-sharing CoO_6 octahedra. The following

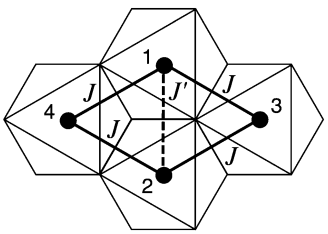

Fig. 35 The structure of the Co_4O_{16} cluster and the network of the exchange parameters.

effective pseudo-spin-1/2 exchange Hamiltonian was used to describe the pattern of low-lying energy levels:

$$\hat{H}_{ex} = -2 \sum_{\alpha=X,Y,Z} [J_\alpha(\hat{\tau}_\alpha^1\hat{\tau}_\alpha^3 + \hat{\tau}_\alpha^1\hat{\tau}_\alpha^4 + \hat{\tau}_\alpha^2\hat{\tau}_\alpha^3 + \hat{\tau}_\alpha^2\hat{\tau}_\alpha^4) + J'_\alpha\hat{\tau}_\alpha^1\hat{\tau}_\alpha^2]. \quad (58)$$

In eqn (58) the two dominant exchange pathways J and J' correspond to the interactions along the edges and the short diagonal of the rhomb, respectively, meanwhile the interactions along the long diagonal are neglected (Fig. 31). The analysis of the INS spectra led us to the following set of parameters: $J_Z = 1.51$ meV, $J_X = 0.70$ meV, $J'_Z = 0.46$ meV, $J'_X = 0.44$ meV, $r = J_X/J_Y = J'_X/J'_Y = 1.6$. Both interactions turned out to be ferromagnetic and anisotropic with $J_Z > J_X$, J_Y and $J'_Z > J'_X, J'_Y$. This set of parameters allows us to reproduce the observed temperature dependence of the magnetic heat capacity and also the experimental χT *vs.* T curve.

The INS technique was also used for the study of the exchange interactions in the more complex pentameric Co^{II} cluster $[Co_3W(D_2O)_2(CoW_9O_{34})_2]^{12-}$, which contains three octahedral and two tetrahedral oxo-coordinated Co^{II} ions.[113] This study revealed two kinds of highly anisotropic exchange interactions in this compound: a ferromagnetic interaction between the octahedral Co^{II} ions and an antiferromagnetic interaction between the octahedral and the tetrahedral Co^{II} ions. The set of parameters of the effective pseudo-spin-1/2 Hamiltonian derived from the analysis of INS spectra was shown to reproduce in a satisfactory manner the susceptibility, magnetization, and INS properties of the compound.

Finally, we should mention the INS investigations of two trimeric Co^{II} clusters: $[Co_3W(D_2O)_2(ZnW_9O_{34})_2]^{12-}$ [114] and $[(NaOH_2)Co_3(H_2O)(P_2W_{15}O_{56})_2]^{17-}$.[115] In these cases the INS experimental data indicate that a model based on anisotropic exchange interactions is insufficient to describe the experiment. Thus, the different orientations of the anisotropic exchange tensors must be taken into account which are correlated with the molecular symmetries of the complexes. Summarizing one can conclude that the INS technique proved to be a very efficient tool for a reliable and unambiguous determination of the parameters involved in the phenomenological pseudo-spin-1/2 Hamiltonian.

6. Conclusions and outlook

The aim of the paper has been to describe in an accessible manner how the orbital degeneracy affects both the exchange interaction and the magnetic anisotropy of molecular magnetic clusters. We have discussed the conceptual aspects of the problem and illustrated how the theoretical approaches and methodology can be applied to describe the magnetic properties of the systems with unquenched orbital angular momentum. We have pointed out that the orbital degeneracy represents a complicated many-side problem. Even if one takes into account all advantages provided by the theoretical approaches to the problem of the orbitally-dependent exchange, the full description of the magnetic and spectroscopic behavior of these complex systems remains a challenge. For this reason we have considered a number of specially

selected model systems that illustrate in a simple but profound manner the main features of the molecular magnets which are related to their orbital degeneracy.

The key topics and conclusions of this review can be summarized as follows:

(1) The major electronic factors controlling the exchange anisotropy have been discussed for dinuclear systems composed by orbitally-degenerate metal ions. The character of this anisotropy was shown to depend on both the electronic configurations and terms of the constituent mononuclear moieties (single-ion crystal field parameters), and on the overall symmetry of the pair. This last aspect applies to taking into account the relative magnitude of the different electron transfer pathways between unfilled d-shells contributing to the kinetic exchange. Thus, the exact form of the exchange Hamiltonian, which in these cases involves both spin and orbital operators, will be specific for each system as it will depend on the exact geometry of the system. This result is in sharp contrast to what happens when we are dealing with non-degenerate metal ions, since in these cases an HDVV spin Hamiltonian, whose form is totally independent from the geometry of the system, is valid. Nevertheless, we have also shown that in some special cases, when the total orbital degeneracy of the pair is equal to the number of the equivalent transfer pathways or when the electron transfer is only efficient within the orbitally nondegenerate electronic subshells, the interaction between the orbitally-degenerate ions becomes orbitally independent and the exchange Hamiltonian takes on a pseudo-Heisenberg spin form. This latter situation is exemplified by the clusters composed of high-spin Co^{II} ions for which the so called Lines model based on the pseudo-Heisenberg Hamiltonian is widely used. In all other cases the exchange interaction between metal ions with unquenched orbital angular momenta proves to be orbitally-dependent and highly anisotropic, even when it couples isotropic (octahedrally coordinated) metal ions;

(2) In the case of strong SO interaction the effective Hamiltonian for a dimer consisting of half-integer spins was projected onto the subspace of low-lying Kramers doublets. In this way, a pseudo-spin-1/2 Hamiltonian was derived. Unlike the commonly accepted phenomenological approaches based merely on the symmetry arguments (such as the Lines model), the described procedure is grounded on microscopic considerations and hence allows us to establish a link between the real parameters of the system and the effective parameters of the pseudo-spin-1/2 Hamiltonian;

(3) A series of molecular magnets based on the orbitally degenerate ions have been analyzed: (i) the magnetic properties of the dinuclear face-sharing bioctahedral unit $[Ti_2Cl_9]^{3-}$ in $Cs_3Ti_2Cl_9$ have been discussed with a special emphasis on the experimentally observed magnetic anisotropy; (ii) the orbitally-dependent exchange is considered in the rare-earth compounds $Cs_3Yb_2Cl_9$ and $Cs_3Yb_2Br_9$ and the origin of surprising isotropy is revealed; (iii) a zig-zag chain composed of the $Co(H_2L)(H_2O)$ units and exhibiting non-collinear spin structure is considered and the nature of SCM behavior of this compound is shown to be a result of orbitally dependent contributions; (iv) a pseudospin-1/2 Hamiltonian approach was applied to the study of the magnetic anisotropy in the trigonal bipyramidal Ni_3Os_2 compound; (v) finally, the pseudospin-1/2 Hamiltonian approach has also been illustrated by studying the inelastic neutron scattering spectra and magnetic susceptibility of polyoxometalates encapsulating Co^{II} clusters of various nuclearities and symmetries. The analysis of these spectroscopic measurements has allowed us to test the validity of the pseudospin-1/2 Hamiltonian approach, demonstrating the presence of anisotropic exchange interactions in these Co^{II} clusters.

Finally, it is worth noting that the importance of the anisotropic terms in the exchange Hamiltonian (mainly coming from the single-ion anisotropy) was understood at the early stage of magnetochemistry. These anisotropic interactions are crucial, for example, for EPR, but, in general, they are rather small in HDVV systems. In the last years the interest in understanding and controlling the magnetic anisotropy in molecular systems has been progressively growing. This situation is due to the discovery of the molecular nanomagnets (SMMs and SCMs) in the 90's, since in these systems the formation of the energy barrier for the reversal of magnetization has shown to be connected to the magnetic anisotropy. Thus, although many efforts have been applied to control the anisotropy barrier in these systems this task remains a challenging goal that requires new approaches. In fact, in the SMMs reported to date the blocking temperatures do not exceed a few Kelvin, which are too low for application of these systems as the data-storage units. Therefore, the design of new SMMs with higher blocking temperatures and thus with higher magnetization reversal barriers represents an important goal in the field of molecular magnetism. Particularly, the increase of the full spin S seemed to be a promising way to design SMMs with higher blocking temperatures. However, as has been recently demonstrated by Waldmann[144] the parameter D_S proves to be proportional to S^{-2} and hence the barrier Δ_b does not rise with the increase of S. Probably for this conceptually important reason the attempts to increase S by the synthesis of big spin-clusters with high values of the ground state spin has not yet produced better SMMs. Furthermore, in order to have ground spin states well-separated in energy from the excited states, one needs also to maximize the size of the exchange interactions. As follows from the present review, one of the promising ways of increasing the magnetic anisotropy in SMMs is to go beyond HDVV systems and to focus on the magnetic clusters composed of orbitally degenerate metal ions that have unquenched orbital angular momenta.[145] As distinguished from the spin-clusters in which the magnitude of the barrier depends mainly on the relatively small ZFS of the ground spin-state, the barrier in the systems comprising metal ions with unquenched orbital angular momenta can be essentially larger. At the same time, more knowledge is required about the relaxation processes in degenerate systems that are undoubtedly faster than in spin systems and, moreover, have specific features due to involvement of the orbital states directly coupled to phonons. In any case, the design of new SMMs based on orbitally degenerate ions seems to be a promising route for reaching higher energy barriers and for enhancing the blocking temperature. In this context, it has been shown that by taking advantage of the strong

magnetic anisotropy of the rare-earth metal ions (mainly lanthanides, but also actinides), one can obtain mononuclear single-molecule magnets exhibiting high energy barriers.[146,147]

As a final comment we would like to underscore the point that the scope of this review did not allow us to discuss several other important questions related to the degeneracy. For example, we did not address the problem of the Jahn–Teller (JT) effect which is an essential part of the theory of the systems exhibiting orbital degeneracy (see books 148 and 149 and refs. therein) and which is expected to play an important role in the study of exchange-coupled systems containing degenerate ions. On the other hand, the discussion of *ab initio* calculations to get additional information about both the exchange and the JT vibronic parameters is also out of the scope of this review. In this respect the reader is referred to a series of the papers of Atanasov *et al.*[150] in which a combined ligand field and DFT analysis of the magnetic anisotropy and JT effect in oligonuclear complexes is described.

Abbreviations

HDVV model	Heisenberg–Dirac–Van Vleck model
SO	spin-orbital
ZFS	zero-field splitting
INS	inelastic neutron scattering
TIP	temperature independent paramagnetism
CT	charge transfer
SMM	single molecule magnet
SCM	single chain magnet
Jahn–Teller effect	JT effect

Acknowledgements

B.T. and K.R.D. gratefully acknowledge financial support from the USA-Israel Binational Science Foundation, BSF (Grant No. 2006498). B.T. thanks the Israel Science Foundation, ISF, for the financial support (grant no. 168/09). K.R.D. is grateful for support of this research by the Department of Energy. A.V.P. and S.I.K. gratefully acknowledge financial support from STCU (project N 5062). J.M.C.J. and E.C. thank Spanish MICINN (CSD2007-00010 CONSOLIDER-INGENIO in Molecular Nanoscience, MAT2007-61584, CTQ-2008-06720 and CTQ-2005-09385), Generalitat Valenciana (PROMETEO program), and the EU (MolSpinQIP project and ERC Advanced Grant SPINMOL) for financial support. We also thank the people that during many years have been collaborating with us in molecular magnetism. Their names appear in this review paper.

References

1 D. Gatteschi, R. Sessoli and J. Villain, *Molecular Nanomagnets*, Oxford University Press, Oxford, 2006.
2 (*a*) K. R. Dunbar and E. Coronado (ed.) *Inorg. Chem.*, 2009, **48**(8), Special issue on Molecular Magnetism; (*b*) E. Coronado and K. R. Dunbar, *Inorg. Chem.*, 2009, **48**, 3293.
3 (*a*) D. Gatteschi and R. Sessoli, *Angew. Chem., Int. Ed.*, 2003, **42**, 268; (*b*) D. Gatteschi and R. Sessoli, *J. Magn. Magn. Mater.*, 2004, **272–276**, 1030.
4 A. Bencini and D. Gatteschi, *Electron Paramagnetic Resonance of Exchange Coupled Systems*, Springer, Berlin, 1990.
5 O. Kahn, *Molecular Magnetism*, VCH, New York, 1993.
6 O. Waldmann, *Coord. Chem. Rev.*, 2005, **249**, 2550.
7 *Magneto-structural Correlation in Exchange Coupled Systems*, ed. R. Willett, D. Gatteschi and O. Kahn, NATO ASI Series C140, Kluwer, Dordrecht, 1985.
8 J. Miller and A. Epstein, *MRS Bull.*, 2000, 21.
9 G. Christou, D. Gatteschi, D. N. Hendrickson and R. Sessoli, *MRS Bull.*, 2000, **25**, 66.
10 R. Sessoli, H.-L. Tsai, A. R. Schake, S. Wang, J. B. Vincent, K. Folting, D. Gatteschi, G. Christou and D. N. Hendrickson, *J. Am. Chem. Soc.*, 1993, **115**, 1804.
11 R. Sessoli, D. Gatteschi, A. Caneschi and M. A. Novak, *Nature*, 1993, **365**, 141.
12 J. M. Clemente-Juan and E. Coronado, *Coord. Chem. Rev.*, 1999, **193–195**, 361.
13 M. Verdaguer, A. Bleuzen, J. Vaissermann, M. Seuileman, C. Desplanches, A. Scuiller, C. Train, G. Gelly, C. Lomenech, I. V. P. Rosenman, C. Cartier and F. Villian, *Coord. Chem. Rev.*, 1999, **190–192**, 1023.
14 (*a*) B. S. Tsukerblat and M. I. Belinsky, *Magnetochemistry and Radiospectroscopy of Exchange Clusters*, Pub. Stiintsa (Acad. Sci. Moldova), Kishinev, 1983 (Rus); (*b*) B. S. Tsukerblat, *Group Theory in Chemistry and Spectroscopy*, Dover, Mineola, New York, 2006.
15 B. S. Tsukerblat, M. I. Belinskii and V. E. Fainzilberg, *Magnetochemistry and Spectroscopy of Transition Metal Exchange Clusters*, in *Soviet Sci. Rev. B*, ed. M. E. Vol'pin, Harwood Acad. Pub., New York, 1987, vol. 9, pp. 337–481.
16 J. J. Borras-Almenar, J. M. Clemente-Juan, E. Coronado, A. V. Palii and B. S. Tsukerblat, *Magnetic Properties of Mixed-Valence Systems: Theoretical Approaches and Applications*, in *Magnetoscience—From Molecules to Materials*, ed. J. Miller and M. Drillon, Willey-VCH, 2001, pp. 155–210.
17 V. Ya. Mitrofanov, A. E. Nikiforov and V. I. Cherepanov, *Spectroscopy of Exchange-Coupled Complexes in Ionic Crystals*, Moskow, Nauka, 1985 (Rus).
18 E. Coronado, R. Georges and B. S. Tsukerblat, *Exchange Interactions: Mechanisms*, in *Localized and Itinerant Molecular Magnetism: From Molecular Assemblies to the Devices*, NATO ASI Series, ed. E. Coronado, P. Delhaes, D. Gatteschi and J. Miller, Kluwer Acad. Publishers, 1996, pp. 65–84.
19 J. M. Clemente, R. Georges, A. V. Palii and B. S. Tsukerblat, *Exchange Interactions: Spin Hamiltonians*, Kluwer Acad. Publishers, 1996, pp. 85–104.
20 R. Bõca, *Theoretical Foundations of Molecular Magnetism*, Elsevier, Amsterdam, 1999.
21 G. Christou, D. Gatteschi, D. N. Hendrickson and R. Sessoli, *MRS Bull.*, 2000, **25**, 66.
22 R. Sessoli, H.-L. Tsai, A. R. Schake, S. Wang, J. B. Vincent, K. Folting, D. Gatteschi, G. Christou and D. N. Hendrickson, *J. Am. Chem. Soc.*, 1993, **115**, 1804.
23 R. Schnalle and J. Schnack, *Int. Rev. Phys. Chem.*, 2010, **29**, 403.
24 G. J. Eppley, H. L. Tsai, N. de Vries, G. Christou and D. N. Hendrickson, *J. Am. Chem. Soc.*, 1995, **117**, 301.
25 S. M. J. Aubin, Z. Sun, I. A. Guzei, A. L. Rheingold, G. Christou and D. N. Hendrickson, *Chem. Commun.*, 1997, 2239.
26 M. R. Cheesman, V. S. Oganesyan, R. Sessoli, D. Gatteschi and A. J. Thomson, *Chem. Commun.*, 1997, 1677.
27 S. L. Castro, Z. Sun, C. M. Grant, J. C. Bollinger, D. N. Hendrickson and G. Christou, *J. Am. Chem. Soc.*, 1998, **120**, 2365.
28 J. C. Goodwin, R. Sessoli, D. Gatteschi, W. Wernsdorfer, A. K. Powell and S. L. Heath, *J. Chem. Soc., Dalton Trans.*, 2000, 1835.
29 C. Boskovic, E. K. Brechin, W. E. Strteib, K. Folting, J. C. Bollinger, D. N. Hendrickson and G. Christou, *J. Am. Chem. Soc.*, 2002, **124**, 3725.
30 C. P. Berlinguette, D. Vaughn, C. Cañada-Vilalta, J.-R. Galán-Mascarós and K. R. Dunbar, *Angew. Chem., Int. Ed.*, 2003, **42**, 1523.
31 H. J. Choi, J. J. Sokol and J. R. Long, *Inorg. Chem.*, 2004, **43**, 1606; S. Wang, J. L. Zuo, H. C. Zhou, H. J. Choi, Y. Ke and J. R. Long, *Angew. Chem., Int. Ed.*, 2004, **43**, 5940.

32 R. Inglis, J. Bendix, T. Brock-Nannestad, H. Weihe and E. K. Brechin, *Chem. Sci.*, 2010, **1**, 631.
33 J. S. Miller, *Polyhedron*, 2009, **28**, 1596.
34 J. S. Miller, *Inorg. Chem.*, 2000, **39**, 4392.
35 J. M. Manriquez, G. T. Yee, R. S. Mclean, A. J. Epstein and J. S. Miller, *Science*, 1991, **252**, 1415.
36 W. R. Entley and G. S. Girolami, *Science*, 1995, **268**, 397.
37 T. Mallah, S. Thiebaut, M. Verdaguer and P. Veillet, *Science*, 1993, **262**, 1554.
38 S. Ferlay, T. Mallah, R. Ouahes, P. Veillet and M. Verdaguer, *Nature*, 1995, **378**, 701.
39 T. Mallah, S. Thiebaut, M. Verdaguer and P. Veillet, *Science*, 1993, **262**, 1554.
40 V. Gadet, T. Mallah, I. Castro, M. Verdaguer and P. Veillet, *J. Am. Chem. Soc.*, 1992, **114**, 9213.
41 D. A. Shultz, R. K. Kumar, S. Bin-Salamon and M. L. Kirk, *Polyhedron*, 2005, **24**, 2876.
42 (*a*) E. Coronado, J. R. Galán-Mascarós, C. J. Gómez-García and V. Laukhin, *Nature*, 2000, **408**, 447; (*b*) E. Coronado and P. Day, *Chem. Rev.*, 2004, **104**, 5419; (*c*) J. Camarero and E. Coronado, *J. Mater. Chem.*, 2009, **19**, 1678.
43 S. Farley, T. Mallah, R. Ouhaes, P. Veillet and M. Verdaguer, *Nature*, 1995, **378**, 701.
44 P. Gütlich, A. Hauser and H. Spiering, *Angew. Chem.*, 1994, **106**, 2109.
45 P. Gütlich, A. Hauser and H. Spiering, *Angew. Chem., Int. Ed. Engl.*, 1994, **33**, 2024.
46 P. Gütlich, Y. Garcia and H. A. Goodwin, *Chem. Soc. Rev.*, 2000, **29**, 419.
47 O. Sato, T. Iyoda, A. Fujishima and K. Hashimoto, *Science*, 1996, **271**, 49.
48 O. Sato, T. Iyoda, A. Fujishima and K. Hashimoto, *Science*, 1996, **272**, 704.
49 M. Verdaguer, *Science*, 1996, **272**, 698.
50 A. Dei, *Angew. Chem., Int. Ed.*, 2005, **44**, 1160.
51 Y. Arimoto, S.-i. Ohkoshi, Z. Jin Zhong, H. Seino, Y. Mizobe and K. Hashimoto, *J. Am. Chem. Soc.*, 2003, **125**, 9240.
52 F. Palacio and J. S. Miller, *Nature*, 2000, **408**, 421.
53 M. Tamura, Y. Nakagawa, D. Shiomi, Y. Nozawa, M. Hosokoshi, M. Ishikawa, M. Takahashi and M. Kinoshita, *Chem. Phys. Lett.*, 1991, **186**, 401.
54 F. Palacio, G. Antorrena, M. Castro, M. Brunel, J. M. Rawson, J. M. Smith, J. N. B. N. Bricklebank, J. Novoa and C. Ritter, *Phys. Rev. Lett.*, 1997, **79**, 2336.
55 I. Fujita, Y. Yeki, T. Takui, T. Kinoshita, K. Itoh, F. Miko, Y. Sawaki, H. Iwamura, A. Izuoka and T. Sugawara, *J. Am. Chem. Soc.*, 1990, **112**, 4074.
56 T. Ishida and H. Iwamura, *J. Am. Chem. Soc.*, 1991, **113**, 4238.
57 A. Rajca, S. Utamapanya and S. Thayumanavan, *J. Am. Chem. Soc.*, 1992, **114**, 1884.
58 N. Nakamura, K. Inoue and H. Iwamura, *Angew. Chem., Int. Ed. Engl.*, 1993, **32**, 873.
59 N. Ventosa, D. Ruiz, C. Rovira and J. Veciana, *Mol. Cryst. Liq. Cryst.*, 1993, **232**, 333.
60 M. Leuenberger and D. Loss, *Nature*, 2001, **410**, 789.
61 D. P. DiVincenzo, *Fortschr. Phys.*, 2000, **48**, 771.
62 W. Wersndorfer and L. Bogani, *Nat. Mater.*, 2007, **6**, 174.
63 (*a*) J. Lehmann, A. Gaita-Arino, E. Coronado and D. Loss, *Nat. Nanotechnol.*, 2007, **2**, 312; (*b*) J. Lehmann, A. Gaita-Ariño, E. Coronado and D. Loss, *J. Mater. Chem.*, 2009, **19**, 1672.
64 F. Troiani, A. Ghirri, M. Affronte, S. Carretta, P. Santini, G. Amoretti, S. Piligkos, G. Timco and R. E. P. Winpenny, *Phys. Rev. Lett.*, 2005, **94**, 207–208.
65 M. Affronte, F. Troiani, A. Ghirri, S. Carretta, P. Santini, V. Corradini, R. Schuecker, C. Muryn, G. Timco and R. E. Winpenny, *Dalton Trans.*, 2006, 2810.
66 M. Affronte, F. Troiani, A. Ghirri, A. Candini, M. Evangelisti, V. Corradini, S. Carretta, P. Santini, G. Amoretti, F. Tuna, G. Timco and R. E. Winpenny, *J. Phys. D: Appl. Phys.*, 2007, **40**, 2999.
67 S. Bertaina, S. Gambarelli, T. Mitra, B. Tsukerblat, A. Müller and B. Barbara, *Nature*, 2008, **453**, 20.
68 P. C. E. Stamp, *Nature*, 2008, **453**, 167.
69 R. E. P. Winpenny, *Angew. Chem., Int. Ed.*, 2008, **47**, 2.
70 D. Stepanenko, M. Trif and D. Loss, *Inorg. Chim. Acta*, 2008, **361**, 3740.
71 A. Ardavan, O. Rival, J. J. L. Morton, S. Blundell, A. M. Tyryshkin, G. A. Timco and E. P. Winpenny, *Phys. Rev. Lett.*, 2007, **98**, 057201.
72 F. K. Larsen, E. J. L. McInnes, H. El Mkami, J. Overgaard, S. Piligkos, G. Rajaraman, E. Rentschler, A. A. Smith, G. M. Smith, V. Boote, M. Jennings, G. A. Timco and R. E. P. Winpenny, *Angew. Chem., Int. Ed.*, 2003, **42**, 101.
73 A. Morello, P. C. E. Stamp and I. S. Tupitsyn, *Phys. Rev. Lett.*, 2006, **97**, 207206.
74 V. V. Dobrovitski, M. I. Katsnelson and B. N. Harmon, *Phys. Rev. Lett.*, 2000, **84**, 3458.
75 G. A. Timco, S. Carretta, F. Troiani, F. Tuna, R. J. Pritchard, C. A. Muryn, E. J. L. McInnes, A. Ghirri, A. Candini, P. Santini, G. Amoretti, M. Affronte and R. E. P. Winpenny, *Nat. Nanotechnol.*, 2009, **4**, 173.
76 G. Mitrikas, Y. Sanakis, C. P. Raptopoulou, G. Kordas and G. Papavassiliou, *Phys. Chem. Chem. Phys.*, 2008, **10**, 743.
77 C. Schlegel, J. van Slageren, M. Manoli, E. K. Brechin and M. Dressel, *Phys. Rev. Lett.*, 2008, **101**, 147203.
78 J. Camarero and E. Coronado, *J. Mater. Chem.*, 2009, **19**, 1678.
79 G. Blondin and J. J. Girerd, *Chem. Rev.*, 1989, **90**, 1359.
80 G. Christou, *Acc. Chem. Res.*, 1989, **22**, 328.
81 S. J. Lippard, *Angew. Chem., Int. Ed. Engl.*, 1991, **30**, 34.
82 K. L. Taft, G. C. Papaefthymiou and S. J. Lippard, *Inorg. Chem.*, 1994, **33**, 1510.
83 J. H. van Vleck, *The theory of electric and magnetic susceptibilities*, Oxford University Press, London, 1932.
84 P. W. Anderson, *Phys. Rev.*, 1959, **115**, 2.
85 P. W. Anderson, in *Solid State Physics*, ed. F. Seitz and D. Turnbull, Academic Press, New York, 1963, vol. 14, p. 99.
86 J. B. Goodenough, *Magnetism and Chemical Bond*, Interscience, New York, 1963.
87 S. Sugano, Y. Tanabe and H. Kamimura, *Multiplets of transition-metal ions in crystals*, Academic Press, New York, London, 1970.
88 J. J. Borrás-Almenar, J. M. Clemente-Juan, E. Coronado, A. V. Palii and B. S. Tsukerblat, *J. Phys. Chem. A*, 1998, **102**, 200.
89 J. J. Borrás-Almenar, J. M. Clemente-Juan, E. Coronado, A. V. Palii and B. S. Tsukerblat, *Phys. Lett. A*, 1998, **238**, 164.
90 J. J. Borrás-Almenar, J. M. Clemente-Juan, E. Coronado, A. V. Palii and B. S. Tsukerblat, *Chem. Phys.*, 2001, **274**, 131.
91 J. J. Borrás-Almenar, J. M. Clemente-Juan, E. Coronado, A. V. Palii and B. S. Tsukerblat, *Chem. Phys.*, 2001, **274**, 145.
92 J. J. Borrás-Almenar, J. M. Clemente-Juan, E. Coronado, A. V. Palii and B. S. Tsukerblat, *J. Chem. Phys.*, 2001, **114**, 1148.
93 J. J. Borrás-Almenar, J. M. Clemente-Juan, E. Coronado, A. V. Palii and B. S. Tsukerblat, *J. Solid State Chem.*, 2001, **159**, 268.
94 J. J. Borras-Almenar, E. Coronado, J. M. Clemente-Juan, A. V. Palii and B. S. Tsukerblat, *Polyhedron*, 2003, **22**, 2521.
95 A. V. Palii, B. S. Tsukerblat, E. Coronado, J. M. Clemente-Juan and J. J. Borrás-Almenar, *J. Chem. Phys.*, 2003, **118**, 5566.
96 A. V. Palii, B. S. Tsukerblat, E. Coronado, J. M. Clemente-Juan and J. J. Borrás-Almenar, *Polyhedron*, 2003, **22**, 2537.
97 A. Palii, B. Tsukerblat, J. M. Clemente-Juan and E. Coronado, *Int. Rev. Phys. Chem.*, 2010, **29**, 135.
98 J. H. Van Vleck, *Revista de Matemática y Fisica Teórica*, Universidad National de Tucumán, vol. 14, 1962, 189.
99 P. M. Levy, *Exchange*, in *Magnetic Oxides*, ed. D. J. Craik, John Wiley, 1975, p. 181.
100 P. M. Levy, *Phys. Rev. A*, 1964, **135**, 155.
101 P. M. Levy, *Phys. Rev. A*, 1969, **177**, 509.
102 M. E. Lines, *J. Chem. Phys.*, 1971, **55**, 2977.
103 A. P. Ginsberg, *Inorg. Chim. Acta, Rev.*, 1971, **5**, 45.
104 B. S. Tsukerblat, A. V. Palii, V. Yu. Mirovitskii, S. M. Ostrovsky, K. Turta, T. Jovmir, S. Shova, J. Bartolome, M. Evangelisti and G. Filoti, *J. Chem. Phys.*, 2001, **115**, 9528.
105 F. Lloret, M. Julve, J. Cano, R. Ruiz-Garcia and E. Pardo, *Inorg. Chim. Acta*, 2008, **361**, 343; A. K. Sharma, F. Lloret and R. Mukherjee, *Inorg. Chem.*, 2007, **46**, 5128.
106 V. Calvo-Perez, S. Ostrovsky, A. Vega, J. Pelikan, E. Spodine and W. Haase, *Inorg. Chem.*, 2006, **45**, 644; S. M. Ostrovsky, K. Falk,

J. Pelikan, D. A. Brown, Z. Tomkowicz and W. Haase, *Inorg. Chem.*, 2006, **45**, 688.
107 W. Van den Heuvel and L. F. Chibotaru, *Inorg. Chem.*, 2009, **48**, 7557.
108 M. Murrie, *Chem. Soc. Rev.*, 2010, **39**, 1986.
109 V. Yan-Zhen Zheng, M. Evangelisti and R. E. P. Winpenny, *Chem. Sci.*, 2011, **2**, 99.
110 J. M. Clemente, H. Andres, M. Aebersold, J. J. Borrás-Almenar, E. Coronado, H. U. Güdel, H. Büttner and C. Kearly, *Inorg. Chem.*, 1997, **36**, 2244.
111 H. Andres, M. Aebersold, H. U. Güdel, J. M. Clemente, E. Coronado, H. Büttner, C. Kearly and M. Zolliker, *Chem. Phys. Lett.*, 1998, **289**, 224.
112 H. Andres, J. M. Clemente-Juan, M. Aebersold, H. U. Güdel, E. Coronado, H. Büttner, C. Kearly, J. Melero and R. Burriel, *J. Am. Chem. Soc.*, 1999, **121**, 10028.
113 H. Andres, J. M. Clemente-Juan, R. Basler, M. Aebersold, H. U. Güdel, J. J. Borrás-Almenar, A. Gaita, E. Coronado, H. Büttner and S. Janssen, *Inorg. Chem.*, 2001, **40**, 1943.
114 J. M. Clemente-Juan, E. Coronado, A. Gaita-Ariño, C. Giménez-Saiz, G. Chaboussant, H.-U. Güdel, R. Burriel and H. Mutka, *Chem.–Eur. J.*, 2002, **8**, 5701.
115 J. M. Clemente-Juan, E. Coronado, A. Gaita-Ariño, C. Giménez-Saiz, H.-U. Güdel, A. Sieber, R. Bircher and H. Mutka, *Inorg. Chem.*, 2005, **44**, 3389.
116 A. V. Palii, B. S. Tsukerblat, E. Coronado, J. M. Clemente-Juan and J. J. Borrás-Almenar, *Inorg. Chem.*, 2003, **42**, 2455.
117 A. V. Palii, *Phys. Lett. A*, 2007, **365**, 116.
118 A. V. Palii, O. S. Reu, S. M. Ostrovsky, S. I. Klokishner, B. S. Tsukerblat, Z.-M. Sun, J.-G. Mao, A. V. Prosvirin, H.-H. Zhao and K. R. Dunbar, *J. Am. Chem. Soc.*, 2008, **130**, 14729.
119 P. L. W. Tregenna-Piggott, D. Sheptyakov, L. Keller, S. I. Klokishner, S. M. Ostrovsky, A. V. Palii, O. S. Reu, J. Bendix, T. B. Nannestad, K. Pedersen, H. Weihe and H. Mutka, *Inorg. Chem.*, 2009, **48**, 128.
120 A. V. Palii, O. S. Reu, S. M. Ostrovsky, S. I. Klokishner, B. S. Tsukerblat, M. Hilfiger, M. Shatruk, A. Prosvirin and K. R. Dunbar, *J. Phys. Chem. A*, 2009, **113**, 6886.
121 K. S. Pedersen, M. Schau-Magnussen, J. Bendix, H. Weihe, A. V. Palii, S. I. Klokishner, S. Ostrovsky, O. S. Reu, H. Mutka and P. L. W. Tregenna-Piggott, *Chem.–Eur. J.*, 2010, **16**, 13458.
122 D. A. Varshalovich, A. N. Moskalev and V. K. Khersonskii, *Quantum Theory of Angular Momentum*, World Scientific, Singapore, 1988.
123 M. Drillon and R. Georges, *Phys. Rev. B*, 1981, **24**, 1278.
124 B. Leuenberger and H. U. Güdel, *Mol. Phys.*, 1984, **51**, 1.
125 A. Ceulemans, L. F. Chibotaru, G. A. Heylen, K. Pierloot and L. G. Vanquickenborne, *Chem. Rev.*, 2000, **100**, 787.
126 B. Briat, O. Kahn, I. Morgenstern-Badarau and J. C. Rivoal, *Inorg. Chem.*, 1981, **20**, 4193.
127 L. J. De Jongh and A. R. Miedema, *Adv. Phys.*, 1974, **23**, 1.
128 R. L. Carlin, *Magnetochemistry*, Springer, Berlin, 1986.
129 A. Maeda and H. Sugimoto, *J. Chem. Soc., Faraday Trans.*, 1986, **2**, 82.
130 S. Hüfner, *Optical Spectra of Transparent Rare Earth Compounds*, Academic, New York, 1978, p. 147.
131 V. S. Mironov, L. F. Chibotaru and A. Ceulemans, *Phys. Rev. B*, 2003, **67**, 014424.
132 A. Furrer, H. U. Güdel and J. Darriet, *J. Less-Common Met.*, 1985, **111**, 223.
133 A. Furrer, H. U. Güdel, H. Blank and A. Heidemann, *Phys. Rev. Lett.*, 1989, **62**, 210.
134 A. Furrer, H. U. Güdel, E. R. Krausz and H. Blank, *Phys. Rev. Lett.*, 1990, **64**, 68.
135 H. U. Güdel, A. Furrer and H. Blank, *Inorg. Chem.*, 1990, **29**, 4081.
136 A. V. Palii, B. S. Tsukerblat, J. M. Clemente-Juan and E. Coronado, *Inorg. Chem.*, 2005, **44**, 3984.
137 Z.-M. Sun, A. V. Prosvirin, H.-H. Zhao, J.-G. Mao and K. R. Dunbar, *J. Appl. Phys.*, 2005, **97**, 10B305.
138 R. J. Glauber, *J. Math. Phys.*, 1963, **4**, 294.
139 M. Hilfiger, M. Shatruk and A. Prosvirin, *Chem. Commun.*, 2008, 5752.
140 C. P. Berlinguette, D. Vaughn, C. Cañada-Vilalta, J.-R. Galán-Mascarós and K. R. Dunbar, *Angew. Chem., Int. Ed.*, 2003, **42**, 1523.
141 P. Albores, L. D. Slep, L. M. Baraldo, R. Baggio, M. T. Garland and E. Rentschler, *Inorg. Chem.*, 2006, **45**, 2361.
142 M. Nishino, Y. Yoshioka and K. Yamaguchi, *Chem. Phys. Lett.*, 1998, **297**, 51.
143 J. J. Borras-Almenar, J. M. Clemente, E. Coronado and B. S. Tsukerblat, *Inorg. Chem.*, 1999, **38**, 6081.
144 O. Waldmann, *Inorg. Chem.*, 2007, **46**, 10035.
145 A. V. Palii, S. M. Ostrovsky, S. I. Klokishner, B. S. Tsukerblat and K. R. Dunbar, *ChemPhysChem*, 2006, **7**, 871; B. Tsukerblat, A. Palii, S. Ostrovsky, S. Kunitsky, S. Klokishner and K. Dunbar, *J. Chem. Theory Comput.*, 2005, **1**, 668.
146 N. Ishikawa, M. Sugita, T. Ishikawa, S. Koshihara and Y. Kaizu, *J. Am. Chem. Soc.*, 2003, **125**, 8694.
147 M. A. AlDamen, J. M. Clemente-Juan, E. Coronado, A. Gaita-Ariño and C. Martí-Gastaldo, *J. Am. Chem. Soc.*, 2008, **27**, 3650.
148 R. Englman, *The Jahn–Teller Effect in Molecules and Crystals*, Wiley, London, 1972.
149 I. B. Bersuker and V. Z. Polinger, *Vibronic Interactions in Molecules and Crystals*, Springer-Verlag, Berlin, 1989; I. B. Bersuker, *The Jahn–Teller Effect*, Cambridge University Press, 2006.
150 M. Atanasov, P. Comba and C. A. Daul, *Inorg. Chem.*, 2008, **47**, 2449; M. Atanasov, P. Comba and C. A. Daul, *J. Phys. Chem. A*, 2006, **110**, 13332; M. Atanasov, C. Busche, P. Comba, F. El Hallak, B. Martin, G. Rajaraman, G. Rajaraman, J. van Slageren and H. Wadepohl, *Inorg. Chem.*, 2008, **47**, 8112.

